Title

Biostratigraphy, magnetostratigraphy, and geochronology of lower Miocene Aoerban strata in Central Inner Mongolia

Authors

Wang, Xiaoming
Li, Qian
Sun, Lu
et al.

Publication Date

2019-03-01

DOI

10.1016/j.palaeo.2018.12.006

Peer reviewed

Palaeogeography, Palaeoclimatology, Palaeoecology 518 (2019) 187–205

Contents lists available at ScienceDirect

Palaeogeography, Palaeoclimatology, Palaeoecology

journal homepage: www.elsevier.com/locate/palaeo

Biostratigraphy, magnetostratigraphy, and geochronology of lower Miocene Aoerban strata in Central Inner Mongolia

Xiaoming Wang[a,b,*], Qian Li[c], Lu Sun[c,d,e], Chenglong Deng[c,d,e], Qiang Li[a,b,f], Wen Dusu[g]

[a] Department of Vertebrate Paleontology, Natural History Museum of Los Angeles County, 900 Exposition Blvd., Los Angeles, CA 90007, USA
[b] Key Laboratory of Vertebrate Evolution and Human Origins of Chinese Academy of Sciences, Institute of Vertebrate Paleontology and Paleoanthropology, Chinese Academy of Sciences, Beijing 100044, China
[c] State Key Laboratory of Lithospheric Evolution, Institute of Geology and Geophysics, Chinese Academy of Sciences, Beijing 100029, China
[d] Institutions of Earth Science, Chinese Academy of Sciences, Beijing 100029, China
[e] College of Earth and Planetary Sciences, University of Chinese Academy of Sciences, Beijing 100049, China
[f] Chinese Academy of Sciences Center for Excellence in Life and Paleoenvironment, Beijing, 100044, China
[g] Museum of Sonit Left Banner, Xilin Gol League, Inner Mongolia 011300, China

ARTICLE INFO

Keywords:
Fossil mammals
Zoogeography
Evolution
China
East Asia
Cenozoic

ABSTRACT

The Aoerban region of central Inner Mongolia, China is an important early Miocene fossil site that contains a diverse mammalian record unrivaled by other Asian sites of similar age. In this paper, we present lithostratigraphic, biostratigraphic, and magnetostratigraphic data from Aoerban Formation to better understand faunal changes between the Xiejian and Shanwangian Chinese Land Mammal ages. With new biochronological constraints, magnetochrons in the Aoerban Formation can be correlated to C6An.2n to C5Cr with an age range of 20.71–16.72 Ma of the Astronomically Tuned Neogene Timescale (ATNTS2012). The strata of the Aoerban region contain a number of important mammalian First Appearance Data, including several morphotypes of deer (Cervidae), horses (*Anchitherium*), pika (*Alloptox*), cricetid rodents (*Megacricetodon*), and possibly the local earliest record of gomphotheres (i.e., the Proboscidea event). Although the ranges for most of these taxa are still poorly known, some of them, alone or in combination, are useful in defining the base the Shanwangian Land Mammal Age. Within this finely calibrated chronologic framework, the faunas of the Aoerban region are important for better understanding mammalian evolution, biogeography, and paleoenvironment.

1. Introduction

Chinese terrestrial records of early Miocene age, and those of the rest of Asia, are exceedingly poor, and as a result, two early Miocene Chinese land mammal ages/stages (LMAs/Ss), the Xiejian and Shanwangian stages, remain poorly defined (Qiu et al., 2013b). Efforts have been made since the 1990s to fill this early Miocene gap, but our state of knowledge remains poor in contrast to better-sampled middle and late Miocene strata. The early Miocene fossil-rich successions of the Aoerban region, first discovered in 2004, stand out because of their abundant vertebrate fossil assemblages, which include both large and small mammals (Wang et al., 2009). A diverse and dense fossil record has been recovered from a section about 50 m thick, the second thickest exposure in a single site of Neogene age in Inner Mongolia, affording opportunities for paleomagnetic studies to further constrain age relationships. The long and continuous section of the Aoerban Formation is the only exposure straddling the Xiejian and Shanwangian Chinese Neogene LMAs, as currently conceived (Qiu et al., 2013b), and plays an important role in characterizing the beginning of Shanwangian. Given this important context, intense efforts during the past decade have led to a refined biostratigraphy and chronology that sheds much needed light on this critical period – time during which Oligocene archaic mammals transitioned into modern forms of the Miocene. In this report, we focus on the biostratigraphy and magnetostratigraphy, and using fossil mammals as constraints, we establish a chronologic framework for the Aoerban Formation.

1.1. Institutional abbreviations

IM, fossil localities of Inner Mongolia; **IVPP**, Institute of Vertebrate Paleontology and Paleoanthropology, Chinese Academy of Sciences, Beijing.

* Corresponding author at: Department of Vertebrate Paleontology, Natural History Museum of Los Angeles County, 900 Exposition Blvd., Los Angeles, CA 90007, USA.
E-mail address: xwang@nhm.org (X. Wang).

https://doi.org/10.1016/j.palaeo.2018.12.006
Received 13 July 2018; Received in revised form 11 December 2018; Accepted 11 December 2018
Available online 18 December 2018
0031-0182/

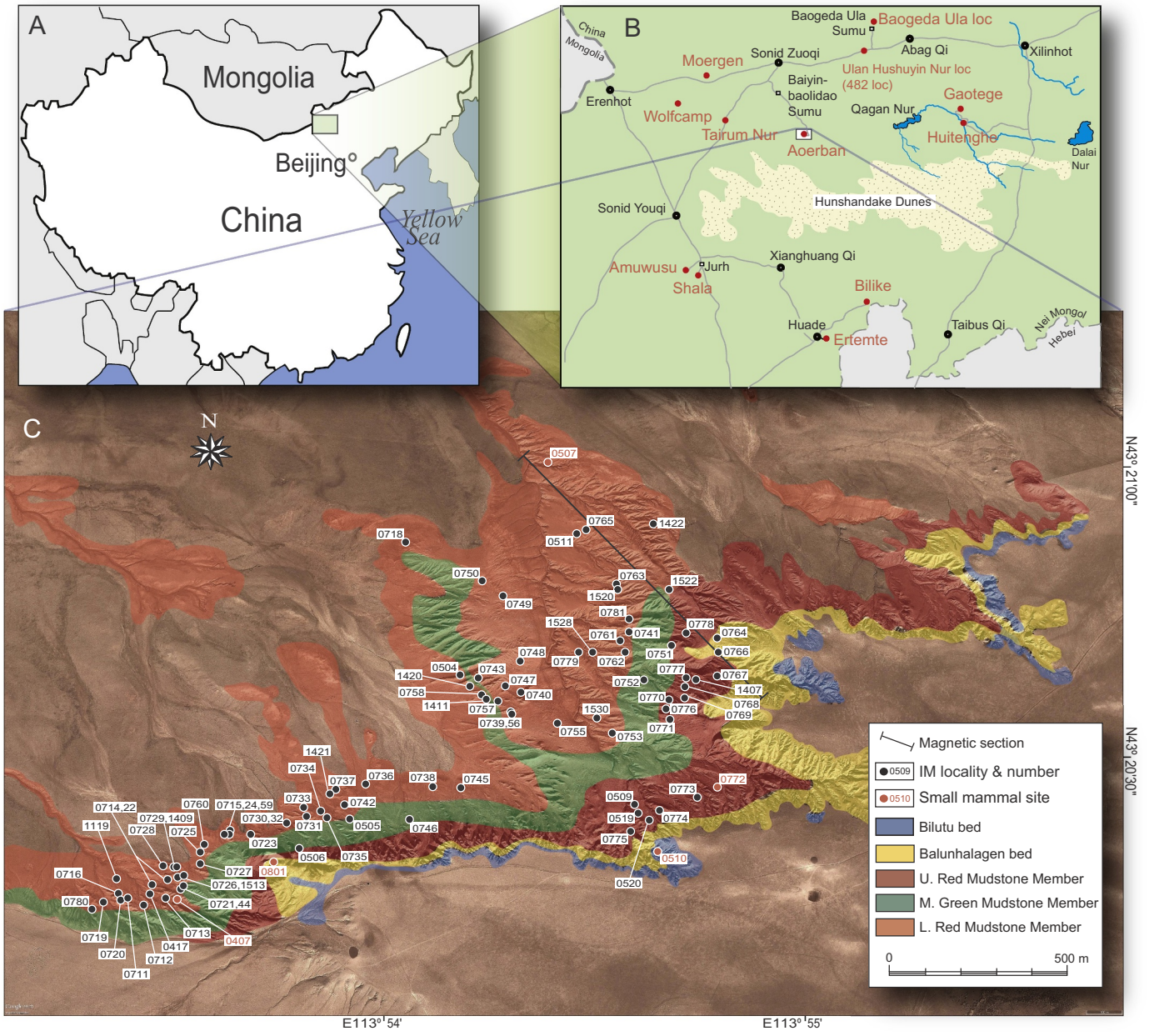

Fig. 1. A, map of China and Mongolia; B, regional map of central Inner Mongolia showing major fossil sites in red; C, geologic map of Aoerban badlands with vertebrate fossil localities plotted on satellite image from Google Earth Pro (2015). Mapping of geologic units follows that of Wang et al. (2009, 2016). See Table 1 for detailed locality information. (For interpretation of the references to color in this figure legend, the reader is referred to the web version of this article.)

2. Geologic setting and lithostratigraphy

Located in Sonid Zuoqi, Xilin Gol Meng (League), central Inner Mongolia (Fig. 1), the Aoerban section consists of three lithologic units, comprising from bottom to top, the Aoerban Formation, the Balunhalagen Bed and the Bilutu Bed (Fig. 1). The Aoerban Formation is continuously exposed in an area of 3 × 2 km^2 (43°20′ to 43°21.5′N, 113°53′ to 113°56′E) (Wang et al., 2009), and mainly consists of mudstones of various colors. Three lithologic units are recognized in the formation, i.e., the Lower Red Mudstone Member, the Middle Green Mudstone Member, and the Upper Red Mudstone Member (Wang et al., 2009). The Middle Green Mudstone Member probably represents a water-logged bed that is likely time-transgressive. The greenish color may be a diagenetic feature, but nonetheless comprises useful marker in the field.

Whereas the Aoerban Formation itself appears to represent essentially continuous deposition, the overlying Balunhalagen Bed, which is characterized by basal conglomeratic sandstones and gravels followed by grayish-yellow and reddish siltstones, cuts deeply into the Aoerban Formation and a prominent disconformity is recognizable throughout the Aoerban badlands. The incision can be several meters deep, and has been formed by coarse-grained fluvial channel deposits. Based on fossil content (from IM0801 wash site), a depositional hiatus of several million years must have existed between the Balunhalagen Bed and the underlying Aoerban Formation. A second major hiatus can be recognized by the contact relationship between the Balunhalagen Bed and the capping Bilutu Bed. The latter is mostly a thin layer of gray gravel deposit draped on top of the Balunhalagen Bed, and is elsewhere composed of grayish-white siltstones mixed with carbonate nodules. Fossils in the Bilutu Bed (from IM0510) may have been reworked from the underlying Balunhalagen Bed, and mixed with younger late Miocene forms.

Table 1
List of fossil localities in Aoerban strata, their GPS locations, and calibrated paleomagnetic ages. See Fig. 1 for location of individual localities. * indicates a lack of a reliable correlation to GPTS.

Loc	Latitude	Longitude	Google Earth elev (m)	Memb. (bed)	pmag age (Ma)	Interpolated to pmag section (m)	Interpolated age (Ma)
IM0510	43.339279	113.910468	1084	Bilutu	6–8	0–2	6–8
IM0764	43.344944	113.912838	1075	Balunh.	8–11	2–5.4	8–11
IM0801	43.339029	113.896773	1074	Balunh.	8–11	2–5.4	8–11
IM0773	43.340720	113.911922	1078	U Red	16.72–18.67	6.1	16.7
IM0775	43.339781	113.909532	1078	U Red	16.72–18.67	6.1	16.7
IM0520	43.340083	113.910194	1078	U Red	16.72–18.67	6.1	16.7
IM0767	43.343920	113.912803	1077	U Red	16.72–18.67	7.1	16.9
IM0772	43.340945	113.912701	1076	U Red	16.72–18.67	8.2	17.0
IM0774	43.340361	113.910529	1076	U Red	16.72–18.67	8.2	17.0
IM0766	43.344586	113.912899	1075	U Red	16.72–18.67	9.3	17.1
IM0519	43.340278	113.909777	1075	U Red	16.72–18.67	9.3	17.1
IM1407	43.343750	113.912056	1074	U Red	16.72–18.67	10.4	17.2
IM0506	43.339310	113.897654	1073	U Red	16.72–18.67	11.4	17.4
IM0769	43.343360	113.911553	1073	U Red	16.72–18.67	11.4	17.4
IM0509	43.340477	113.909689	1072	U Red	16.72–18.67	12.5	17.5
IM0778	43.345139	113.911724	1072	U Red	16.72–18.67	12.5	17.5
IM0768	43.343640	113.911615	1071	U Red	16.72–18.67	13.6	17.6
IM0776	43.343029	113.910973	1071	U Red	16.72–18.67	13.6	17.6
IM0770	43.343278	113.911028	1070	U Red	16.72–18.67	14.7	17.8
IM0771	43.342752	113.911028	1070	U Red	16.72–18.67	14.7	17.8
IM0777	43.343889	113.911635	1070	U Red	16.72–18.67	14.7	17.8
IM0751	43.344777	113.911226	1067	U Red	16.72–18.67	17.9	18.2
IM0505	43.340133	113.899382	1065	U Red	16.72–18.67	20.0	18.4
IM1522	43.346389	113.911111	1064	U Red	16.72–18.67	21.1	18.5
IM0738	43.341000	113.902340	1063	U Red	16.72–18.67	22.2	18.7
IM0745	43.340945	113.903391	1063	U Red	16.72–18.67	22.2	18.7
IM0746	43.340112	113.901527	1071	M Green	18.67–19.36	18.1	18.7
IM0752	43.343835	113.910112	1063	M Green	18.67–19.36	22.0	19.4
IM0723	43.339695	113.895776	1062	L Red	19.36–20.71	21.1	19.4
IM0753	43.342414	113.908835	1062	L Red	19.36–20.71	21.1	19.4
IM0755	43.342639	113.906861	1062	L Red	19.36–20.71	21.1	19.4
IM0735	43.340221	113.898501	1061	L Red	19.36–20.71	22.2	19.4
IM0742	43.340416	113.899170	1061	L Red	19.36–20.71	22.2	19.4
IM0730	43.339975	113.897087	1060	L Red	19.36–20.71	23.3	19.5
IM0736	43.340778	113.900024	1060	L Red	19.36–20.71	23.3	19.5
IM0739	43.342889	113.905140	1060	L Red	19.36–20.71	23.3	19.5
IM0741	43.345197	113.909614	1060	L Red	19.36–20.71	23.3	19.5
IM0743	43.343944	113.903945	1060	L Red	19.36–20.71	23.3	19.5
IM0747	43.343695	113.904949	1060	L Red	19.36–20.71	23.3	19.5
IM0756	43.342947	113.905140	1060	L Red	19.36–20.71	23.3	19.5
IM0757	43.343278	113.904696	1060	L Red	19.36–20.71	23.3	19.5
IM0758	43.343445	113.904054	1060	L Red	19.36–20.71	23.3	19.5
IM1411	43.343278	113.904333	1060	L Red	19.36–20.71	23.3	19.5
IM0407	43.338029	113.893167	1059	L Red	19.36–20.71	24.4	19.5
IM0731	43.340194	113.897722	1059	L Red	19.36–20.71	24.4	19.5
IM0732	43.340027	113.897026	1059	L Red	19.36–20.71	24.4	19.5
IM0734	43.340279	113.898194	1059	L Red	19.36–20.71	24.4	19.5
IM0740	43.343531	113.905502	1059	L Red	19.36–20.71	24.4	19.5
IM0781	43.345528	113.909552	1059	L Red	19.36–20.71	24.4	19.5
IM1530	43.342777	113.908333	1059	L Red	19.36–20.71	24.4	19.5
IM1420	43.343611	113.903778	1059	L Red	19.36–20.71	24.4	19.5
IM0715	43.339805	113.894997	1058	L Red	19.36–20.71	25.5	19.6
IM0724	43.339750	113.894977	1058	L Red	19.36–20.71	25.5	19.6
IM0727	43.339002	113.893973	1058	L Red	19.36–20.71	25.5	19.6
IM0744	43.338360	113.893447	1058	L Red	19.36–20.71	25.5	19.6
IM0748	43.344360	113.905440	1058	L Red	19.36–20.71	25.5	19.6
IM0749	43.346222	113.904812	1058	L Red	19.36–20.71	25.5	19.6
IM0750	43.346669	113.904054	1058	L Red	19.36–20.71	25.5	19.6
IM0759	43.339723	113.894860	1058	L Red	19.36–20.71	25.5	19.6
IM0761	43.344917	113.909252	1058	L Red	19.36–20.71	25.5	19.6
IM0762	43.344613	113.909450	1058	L Red	19.36–20.71	25.5	19.6
IM0763	43.346553	113.909142	1058	L Red	19.36–20.71	25.5	19.6
IM1520	43.346389	113.909167	1058	L Red	19.36–20.71	25.5	19.6
IM0713	43.338056	113.892914	1057	L Red	19.36–20.71	26.6	19.7
IM0721	43.338333	113.893365	1057	L Red	19.36–20.71	26.6	19.7
IM0725	43.339306	113.894000	1057	L Red	19.36–20.71	26.6	19.7
IM0726	43.338586	113.893283	1057	L Red	19.36–20.71	26.6	19.7
IM0737	43.340863	113.898863	1057	L Red	19.36–20.71	26.6	19.7
IM0760	43.339443	113.894164	1057	L Red	19.36–20.71	26.6	19.7
IM1421	43.340778	113.898667	1057	L Red	19.36–20.71	26.6	19.7
IM1513	43.338639	113.893472	1057	L Red	19.36–20.71	26.6	19.7
IM0504	43.344005	113.903214	1056	L Red	19.36–20.71	27.6	19.7

(*continued on next page*)

Table 1 (*continued*)

Loc	Latitude	Longitude	Google Earth elev (m)	Memb. (bed)	pmag age (Ma)	Interpolated to pmag section (m)	Interpolated age (Ma)
IM0711	43.338087	113.891336	1056	L Red	19.36–20.71	27.6	19.7
IM0712	43.338002	113.892081	1056	L Red	19.36–20.71	27.6	19.7
IM0717	43.338196	113.892306	1056	L Red	19.36–20.71	27.6	19.7
IM0729	43.338859	113.893030	1056	L Red	19.36–20.71	27.6	19.7
IM0733	43.340389	113.897613	1056	L Red	19.36–20.71	27.6	19.7
IM0714	43.338418	113.892306	1055	L Red	19.36–20.71	28.7	19.8
IM0716	43.338196	113.891083	1055	L Red	19.36–20.71	28.7	19.8
IM0719	43.337971	113.890612	1055	L Red	19.36–20.71	28.7	19.8
IM0720	43.338056	113.891165	1055	L Red	19.36–20.71	28.7	19.8
IM0722	43.338613	113.892777	1055	L Red	19.36–20.71	28.7	19.8
IM0780	43.337834	113.890223	1055	L Red	19.36–20.71	28.7	19.8
IM1409	43.338917	113.892944	1055	L Red	19.36–20.71	28.7	19.8
IM0728	43.338917	113.892695	1054	L Red	19.36–20.71	29.8	19.9
IM1422	43.348306	113.910583	1054	L Red	19.36–20.71	29.8	19.9
IM1528	43.344611	113.908194	1054	L Red	19.36–20.71	29.8	19.9
IM1119	43.338528	113.890972	1052	L Red	19.36–20.71	32.0	20.0
IM0779	43.344641	113.907667	1051	L Red	19.36–20.71	33.1	20.0
IM0718	43.347779	113.901137	1050	L Red	19.36–20.71	34.2	20.1
IM0765	43.348168	113.907947	1046	L Red	19.36–20.71	38.5	20.3
IM0511	43.348093	113.907640	1045	L Red	19.36–20.71	39.6	20.4
IM0507	43.350197	113.906465	1040	L Red	19.36–20.71	45.1	20.7

3. Materials and methods

Our paleomagnetic section at Aoerban begins at 43°20′35.5″N, 113°54′51.5″E and ends at 43°21′01.5″N, 113°54′20.2″E. Samples were oriented by magnetic compass in the field and were taken at 10–20 cm intervals depending on lithology, yielding 266 sampling levels. One block sample was taken from each sampling level. Five sets of sister specimens (2-cm cubic) for each sample were obtained from these block samples in the laboratory. See Supplementary Material for additional descriptions on the methods for mineral magnetism and paleomagnetic measurements.

All fossils are housed in the Institute of Vertebrate Paleontology and Paleoanthropology (IVPP), Chinese Academy of Sciences, Beijing, China. Because all Aoerban beds are flat lying, elevations of individual localities are used as a primary tool for interpolation; each locality is assigned an elevation (Table 1) using the built-in calibration of Google Earth Pro (Version 7.1.1557) (2015). The measurements for magnetic and biostratigraphic sections are done independently, and their integration can be another source of uncertainty.

3.1. Mineral magnetic measurements

A total of 194 specimens were selected to measure anisotropy of magnetic susceptibility (AMS) using a KLY-4s Kappabridge (Agico Ltd., Brno) before thermal demagnetization was conducted. The susceptibility tensor for each specimen was calculated from measurements in 15 positions using the method described by Jelinek (1978). Other mineral magnetic measurements, including high-temperature magnetic susceptibilities (χ–T curves), hysteresis loops, isothermal remnant magnetization (IRM) acquisition, and DC field demagnetization of the saturated IRM (SIRM), were made on representative specimens.

χ–T curves were measured at a frequency of 976 Hz using a MFK1-FA with a CS-4 high-temperature furnace (Agico Ltd., Brno). To avoid oxidization during heating, the specimens were heated in an argon atmosphere.

Stepwise thermal demagnetization of three orthogonal component IRM was further used to characterize the magnetic mineralogy. Selected specimens were magnetized in successively smaller fields along three mutually orthogonal axes (Lowrie, 1990), which are 2.5 T along the Z-axis, 0.5 T along the Y-axis, 0.05 T along the X-axis, respectively, to get a composite IRM, using a 2G Enterprises Pulse Magnetizer (2G660). These specimens were then subjected to progressive thermal demagnetization up to 680 °C at 10–50 °C intervals.

Hysteresis loops and IRM acquisition and its back-field demagnetization characteristics were measured at room temperature using a MicroMag 3900 Vibrating Sample Magnetometer (VSM) (Princeton Measurements Corp., USA). The magnetic field was cycled between ± 1.5 T. Saturation magnetization (M_s), saturation remnance (M_{rs}), and coercivity (B_c) were determined after the correction for paramagnetic contribution identified from the slope at high fields. Specimens were then demagnetized in alternating fields (AFs) up to 1.5 T, and a SIRM was imparted from 0 to 1.5 T also using the MicroMag 3900 VSM. The SIRM was then demagnetized in a stepwise backfield up to −1.0 T to obtain the coercivity of remnance (B_{cr}). The IRM acquisition curves of the selected specimens were then analyzed using the MAG-MIX package of Tauxe (1998) to determine the coercivity distributions.

3.2. Paleomagnetic measurements

One to five specimens from each sampling level were selected for paleomagnetic measurements, which were subjected to progressive thermal demagnetization, AF demagnetization, or hybrid demagnetization. All of the methods were capable of isolating the characteristic remnant magnetization (ChRM) after removal of soft secondary component of magnetization. After each step, the remnance was measured on a three-axis cryogenic magnetometer (2G Enterprises, USA) installed in field-free space (< 300 nT).

Demagnetization results were evaluated by orthogonal diagrams (Zijderveld, 1967). The principal component analyses (PCA) were done using the PaleoMag software (v. 3.1.0 d40) developed by Craig H. Jones and Joya Tetreault. The ChRM directions were determined with linear least squares fitting (Kirschvink, 1980) through the origin by using at least four continuous steps of demagnetization and with a maximum angular deviation (MAD) usually smaller than 15°.

4. Magnetic results

4.1. Anisotropy of magnetic susceptibility (AMS)

The AMS technique provides valuable information on the depositional processes (Tarling and Hrouda, 1993). The magnetic foliation (F) was found to be larger than the magnetic lineation (L) (Fig. 2), which indicates that the AMS ellipsoid of the studied section is oblate. Most

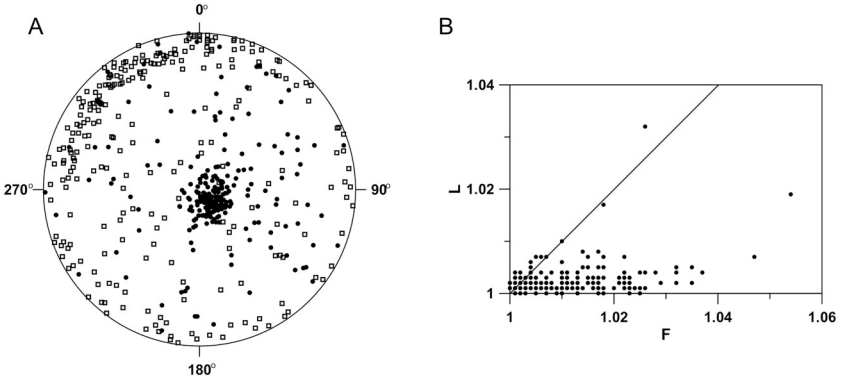

Fig. 2. Anisotropy of magnetic susceptibility (AMS) of samples from the Aoerban section. A, Stereographic projection of principal susceptibility axes of K_{max} (open squares) and K_{min} (solid circles); B, magnetic lineation (L) versus magnetic foliation (F).

minimum susceptibility axes (K_{min}) of the AMS ellipsoid are close to the vertical and perpendicular to the bedding plane. Most maximum axes (K_{max}) are close to the horizontal and parallel to the bedding plane. The AMS results are typical for a primary sedimentary magnetic fabric, indicating that the Aoerban sedimentary sequence has not been disturbed since deposition.

4.2. High-temperature magnetic susceptibility (χ–T curves)

χ–*T* curves have been widely used to determine changes in magnetic mineral composition of natural samples during heat treatment (Deng et al., 2001; Roberts et al., 1995). All χ–*T* curves are characterized by a major drop in magnetic susceptibility at about 585 °C (Fig. 3), the Curie point of magnetite. This behavior indicates that magnetite is the major contributor to the susceptibility. Some specimens show heating curves with a drop of magnetic susceptibility between 275–300 °C and ~450 °C, which is interpreted as the conversion of metastable ferrimagnetic maghemite to weakly magnetic hematite (Stacey and Banerjee, 1974). Hematite is another important carrier of the natural remanence in the Aoerban sediments suggested by progressive thermal demagnetization analyses. However, hematite is not well expressed in the χ–*T* curves because its weak susceptibility is masked by the much stronger contributions from magnetite and maghemite. All selected specimens exhibit cooling curves showing an increase in magnetic susceptibility when cooled below 585 °C. The significantly enhanced susceptibility after thermal treatment is mainly attributed to the formation of magnetite grains from the transformation of iron-containing silicates/clays or to the formation of magnetite by reduction due to the burning of organic matter (Deng et al., 2001).

4.3. Thermal demagnetization of three-component isothermal remanent magnetization (IRM)

Stepwise thermal demagnetization of the three orthogonal

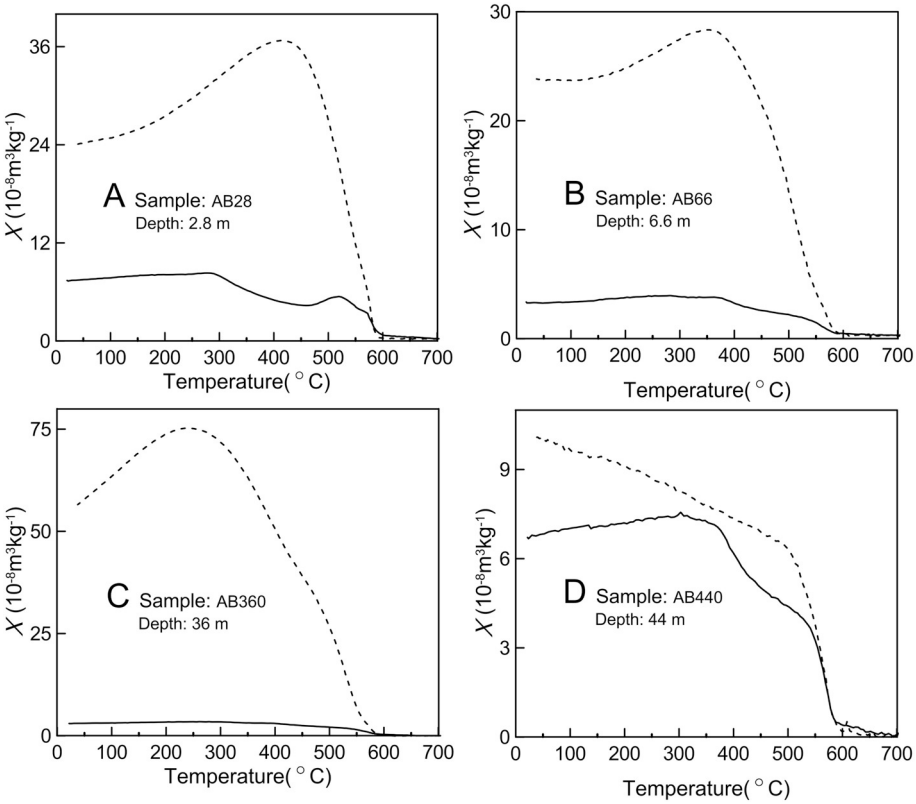

Fig. 3. High-temperature magnetic susceptibility (χ–*T* curves). The solid (dashed) lines represent heating (cooling) curves.

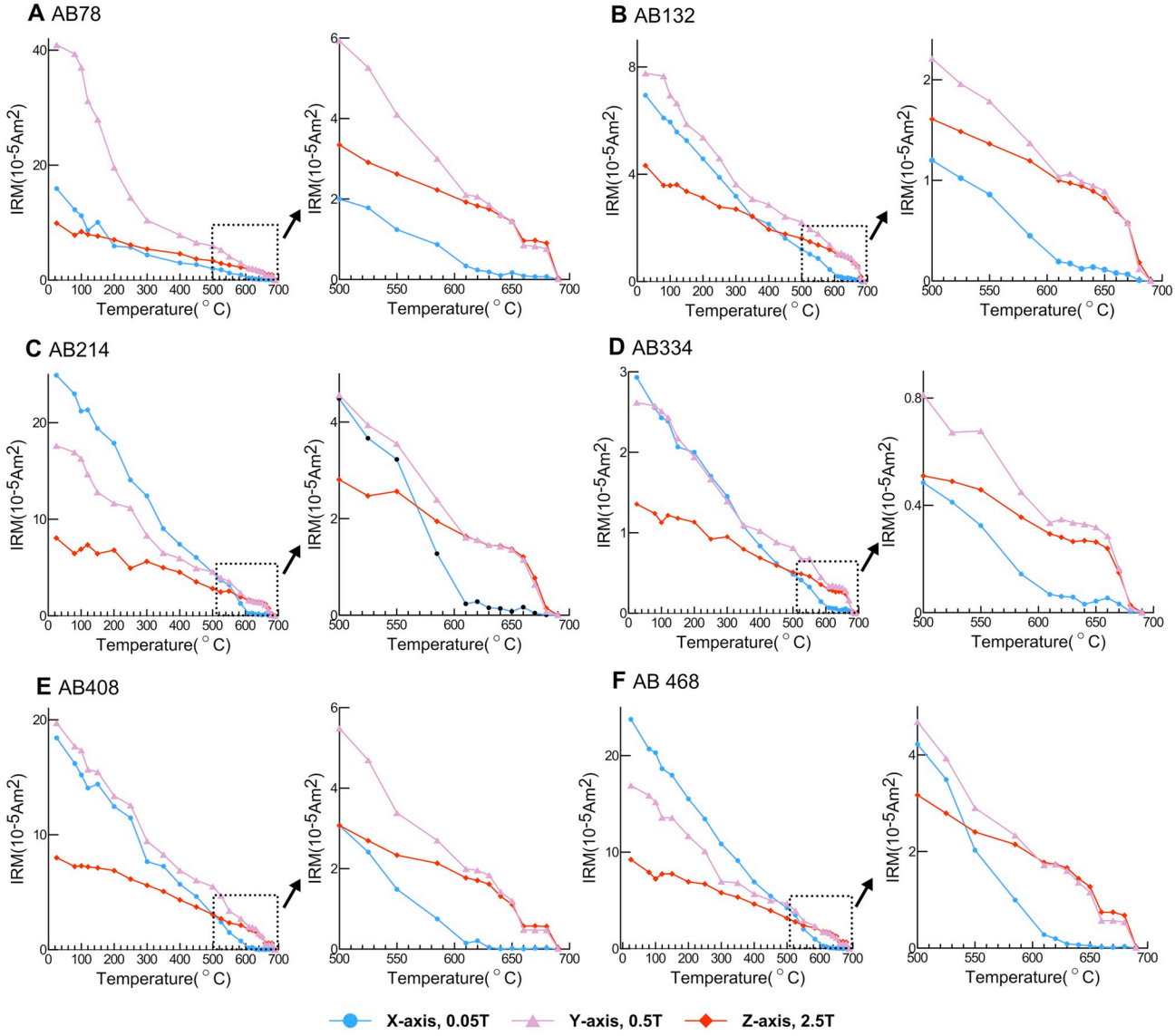

Fig. 4. Progressive thermal demagnetization of a three-component IRM (Lowrie, 1990) produced by magnetizing specimens in 2.5, 0.5 and 0.05 T along the *Z*-, Y- and X-axes, respectively.

component IRM (Lowrie, 1990) is a powerful method to identify the magnetic mineral assemblage of a sample (e.g., Deng et al., 2013; Tauxe, 2010). Fig. 4 shows the thermal demagnetization curves of three-component IRM of selected specimens. The low-coercivity component shows an unblocking temperature of 610 °C, indicative of the presence of partially oxidized magnetite. The medium- and high-coercivity components show an unblocking temperature of 680–690 °C, indicating the presence of hematite. These behaviors suggest that magnetite and hematite are the remanence carriers of the Aoerban specimens.

4.4. Hysteresis properties and IRM acquisition curves

Hysteresis loops, IRM acquisition curves and their component analysis of coercivity distributions (Fig. 5) are also used to assess the magnetic mineralogy. All the selected specimens show hysteresis loops closed above 0.3 T (Figs. 5A, D, G, J, M, P), suggesting the predominance of low-coercivity phases.

The selected specimens yield similar IRM acquisition curves (Figs. 5B, E, H, K, N, Q). The rapid rise below 100 mT indicates the presence of magnetically soft components, such as magnetite and/or maghemite. > 85% of the 1.5 T IRM (hereafter termed SIRM) was acquired below an inducing field of 0.3 T, implying the dominance of low-coercivity magnetic minerals.

S-ratio is the absolute value of the IRM remaining after exposure to a reversed field of 0.3 T divided by SIRM (King and Channell, 1991; Verosub and Roberts, 1995), that is, *S*-ratio = $-\mathrm{IRM}_{-0.3\mathrm{T}}/\mathrm{SIRM}$. The high values of *S*-ratio (generally > 0.8) (Figs. 5B, E, H, K, N, Q) further suggest the dominance of low-coercivity magnetic phases.

Component analyses were conducted on IRM curves using the method of Tauxe (1998). Four of the six selected specimens reveal a one-humped distribution with peak coercivities ranging from 30 to 40 mT (Figs. 5C, I, L, O). This behavior indicates that low-coercivity magnetic minerals are the dominant carriers of remanence. Two of the selected specimens show a two-humped distribution (Figs. 5F, R). The first component has lower coercivities (42–52 mT), while the second component has higher coercivities (121–128 mT).

Considering the above mineral magnetic data (Figs. 3–5), we conclude that the low-coercivity component is assigned to magnetite, and the high-coercivity component represents hematite. In addition, the values of M_{rs}/M_s versus B_{cr}/B_c when plotted on a Day diagram (Day et al., 1977) indicate that the magnetite grain sizes are predominantly pseudo-single domain (Fig. 6).

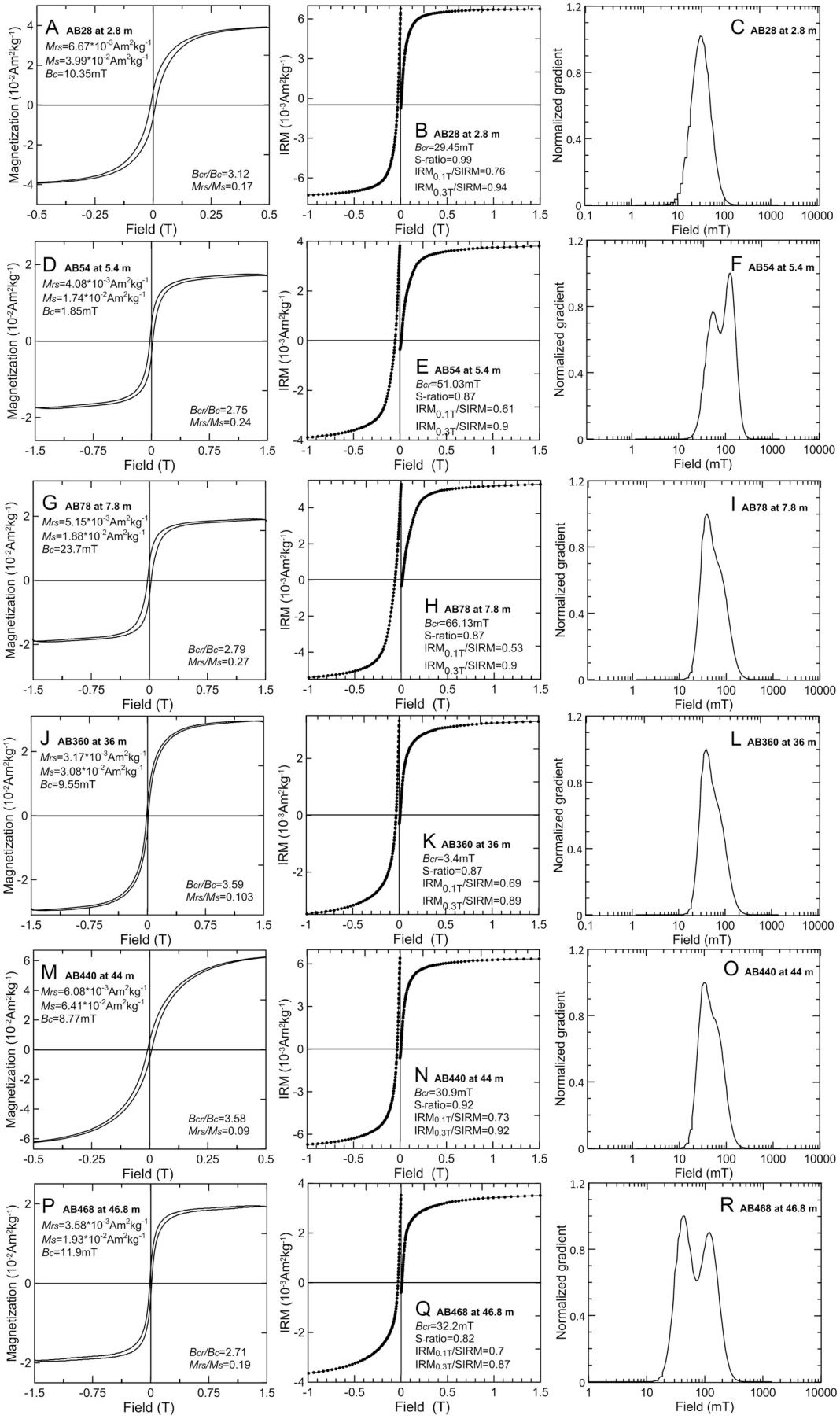

(caption on next page)

Fig. 5. Hysteresis loops after slope correction for paramagnetic contribution (A, D, G, J, M, P), isothermal remanent magnetization (IRM) acquisition and back-field demagnetization curves (B, E, H, K, N, Q), and IRM component analysis of coercivity distributions (C, F, I, L, O, R).

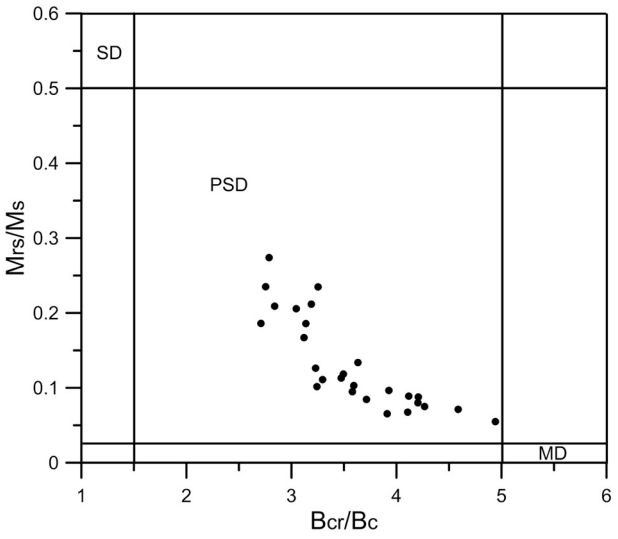

Fig. 6. Day diagram (Day et al., 1977) of hysteresis parameters for representative samples of the Aoerban section. SD, single domain; PSD, pseudo-single domain; and MD, multi-domain.

4.5. Paleomagnetic results

The intensity of the natural remanent magnetization (NRM) of the specimens was usually in the orders of 10^{-4}–10^{-6} A/m. Representative demagnetization diagrams are shown in Fig. 7. Progressive thermal or hybrid demagnetization successfully isolated the characteristic remanent magnetization (ChRM) components after removing one or two soft components of magnetization.

Demagnetization results of representative specimens (Fig. 7) indicate that the high-stability ChRM component of most specimens was separated between 300 °C and 550–610 °C (Figs. 7G, J, K, L, O) or between 20 mT and 60 mT (Figs. 7A, B, F, H, I, M). However, for some specimens the high-stability ChRM component persists up to 640–680 °C (Figs. 7C, D, E, N). The decay curves of the NRM also show that nearly complete demagnetization is achieved at 585–620 °C or 680 °C, or at 60 mT (Fig. 8). These behaviors document that magnetite and hematite dominate the ChRM carriers in the Aoerban sediments. After progressive demagnetization, 126 specimens, which represent 126 sampling levels, from 266 sampling levels (47%) gave reliable characteristic remanence directions, including 15 and 111 specimens with ChRMs carried by hematite and magnetite, respectively.

The virtual geomagnetic pole (VGP) latitudes were calculated from the ChRM data (Fig. 9). These VGP latitudes were subsequently used to define the succession of magnetic polarity events in the Aoerban section. Fifteen magnetozones are recognized in the Aoerban section: eight with normal polarity (N1 to N8), and seven with reverse polarity (R1 to R7) (Fig. 9H).

5. Biostratigraphy

Because of the highly fossiliferous nature of the Aoerban Formation, we attempted to build a complete biostratigraphy by tying each fossil to a locality (a certain amount of aggregation was practiced by individual collectors, which can be as wide as tens of meters in lateral extent). As is often the case, topography plays a role in concentrating fossils weathering out of the ground. As shown in Fig. 10, nearly the entire Aoerban exposure is fossiliferous, with the upper part of the Lower Aoerban red beds having the densest records. To a certain extent, this distribution is probably related to relative flatness of exposure, with steeper exposures along the southern rim of the Aoerban badland having far fewer fossil localities compared to the gentler ground away from the vertical escarpments.

We present a biostratigraphy of the Aoerban strata (Fig. 10). Although major stratigraphic divisions (colored stratigraphic columns in Fig. 10) are straight forward, correlation of individual localities is less precise within members of the Aoerban Formation, which usually lack distinct marker beds. Because all Aoerban beds are flat lying, we choose to use elevations of individual localities as a primary tool for correlation. Each locality is assigned an elevation (Table 1) using the built-in calibration of Google Earth Pro (Version 7.1.1557) (2015).

Our new stratigraphic scheme based on Google Earth Pro is somewhat different from that in our first attempt (Wang et al., 2009:fig. 3). Whereas the relative stratigraphic positions for fossil sites in close proximity are reasonably reliable, we caution that error ranges can be much greater for fossil sites that are hundreds of meters from each other.

6. Biochronology

The systematics and biochronology of rodents from Inner Mongolia were recently monographed by Qiu and Li (2016) (see Faunas below for more discussion). The other small mammals (Insectivora and Lagomorpha) were based on Wang et al. (2009:Table 1) and Qiu et al. (2013a). The following are additional comments on large mammals that can contribute to age assessments.

6.1. Ligeromeryx/Lagomeryx/Stephanocemas

An abundant record of early lagomerycid deers are present in the Aoerban Formation, including isolated antlers, teeth and postcrania (IVPP V24991, V24992, V24993, Figs. 11C–H). These small deers have a protoantler morphology roughly in similar stage of evolution as Ligeromeryx, Lagomeryx and Stephanocemas (Azanza and Ginsburg, 1997). While a more detailed study is under way, these small deers potentially have important biochronologic implications as the first and most basal cervid in East Asia. Other early Miocene basal cervid records include the Sihong Fauna in Jiangsu Province (Li et al., 1983) and Shanwang in Shandong Province (Young, 1937). Nevertheless, the Aoerban forms are both earlier and more primitive in morphology and have the potential to shed lights in early evolution and biogeography of basal cervids.

6.2. Euprox/Dicrocerus

Fragmentary, bifurcate antlers with a rudimentary bur from IM1520 (IVPP V24999) and IM1522 (IVPP V25000) (Figs. 11J, K) indicate the presence of a small deer different from the crowned-antlered forms such as Ligeromeryx/Lagomeryx/Stephanocemas above. These primitive deers typically occur much later in the middle Miocene, and their presence in Aoerban Formation is of chronological significance.

6.3. Anchitherium sp.

As an immigrant to Eurasia from North America, Anchitherium likely have arrived in Asia first before reaching Europe. Yet, much of the fossil records are from Europe, including some of the earliest known occurrences (see Forstén, 1991), possibly because Europe may have been a preferred region for these browsing horses. In Asia, records of Anchitherium are rare, most of them in middle Miocene basins. Chow and Hu (1956) presented the first East Asian early Miocene record, A.

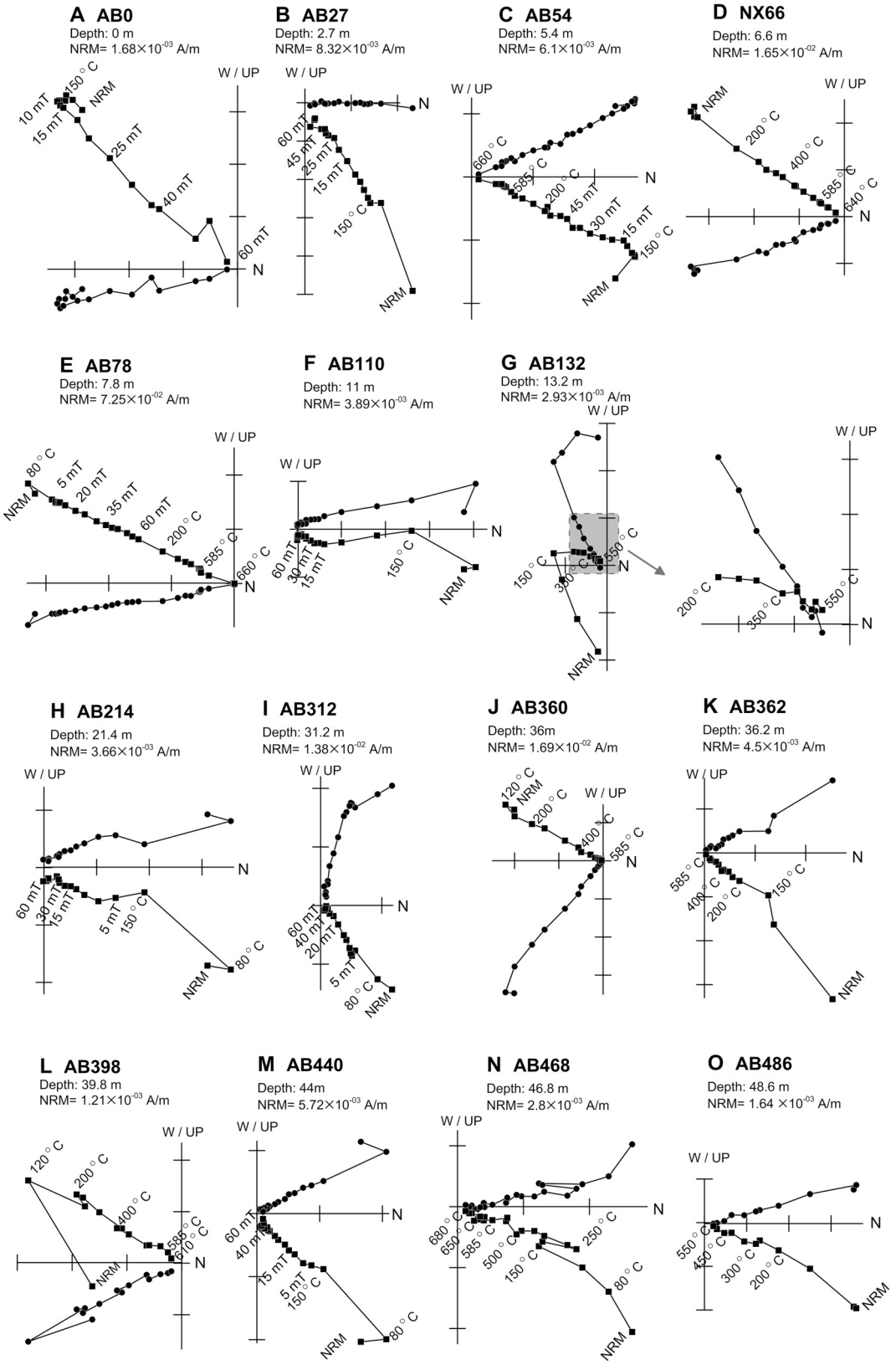

Fig. 7. Orthogonal vector projections of representative progressive thermal and alternating field (AF) demagnetization. The solid circles (squares) represent the horizontal (vertical) planes. The numbers refer to the temperatures in ˚C or alternating fields in mT. NRM is the natural remanent magnetization. Inset to the right of G shows an enlarged view of the demagnetization results at higher temperatures.

aurelianense, from the Shanwangian Fangshan Fauna in Jiangsu Province. This was followed by records from the nearby Sihong Fauna, also in Jiangsu Province (Li et al., 1983; Qiu and Qiu, 2013). More recently, Miyata and Tomida (2010) summarized another Japanese early Miocene record of Anchitherium aff. A. gobiense from the Kani Basin.

Our Lower Aoerban Anchitherium is probably the earliest East Asian

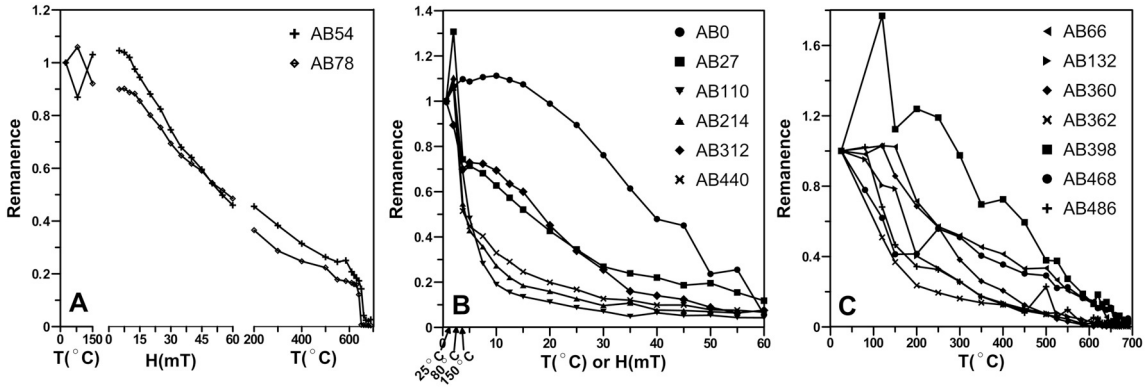

Fig. 8. Decay curves of the NRM for representative specimens as shown in Fig. 7. A, hybrid demagnetization curves for specimens with ChRMs carried by hematite; B, hybrid demagnetization curves for specimens with ChRMs presumably carried by magnetite; C, thermal demagnetization curves for specimens with the ChRMs carried by magnetite or hematite.

record. With a calibrated age of 17.2 Ma for IM1407 loc and 18.5 Ma for IM1522 loc (IVPP V 24990, astragalus, Fig. 11B), our new records are somewhat later than the earliest European occurrences (MN3, ~18–20 Ma). The two teeth (IVPP V 24989) from IM1407 (Fig. 11A), however, are too fragmentary to permit a detailed comparison. Their size seems large, in the range of middle Miocene A. gobiense (Colbert, 1939), and is consistent with the suspicion that eastern Asia may have had early diversifications not previously recognized (Miyata and Tomida, 2010).

6.4. Chalicotheriidae

Isolated foot bones of a chalicothere are found in five localities (Table 2; IVPP V25001 in Figs. 11L, M). Unique phalanx morphologies unambiguously identify these as chalicotheres. Establishing the presence of chalicotheres in Chinese early Miocene, Qiu et al. (1998) described a new species of schizotheriine, Phyllotillon huangheensis, and an old adult of a Chalicotheriinae indet. from the early Miocene strata of Lanzhou Basin. However, both taxa from Lanzhou lack postcranial elements and a detailed comparison is not possible.

6.5. Proboscidea

Two sites, IM0772 (IVPP V24998; Fig. 11I) and 0774, in the Upper Aoerban red bed yielded dental fragments of a proboscidean. Thick enamels and bunodont structures indicate a gomphothere. The exact nature of Aoerban proboscidean awaits more diagnostic materials, although possibilities exist that these surface finds could be eroded from the overlying Balunhalagen Beds (no proboscidean has been recovered from the Balunhalagen Beds).

The First Appearance Datum (FAD) of proboscideans (Proboscidea Datum) (Tassy, 1989) in East Asia is poorly documented. Chinese early Miocene occurrences include Xiacaowan in Jiangsu Province (Chow, 1959) and Danghe (Tabenbuluk) in Gansu Province (Wang and Qiu, 2002), both Shanwangian in age. Previous mentions of early proboscideans from the Zhangjiaping local fauna (Xiejian age) of Lanzhou Basin, Gansu Province (Qiu, 1989; Qiu and Qiu, 1995) was cast in doubt (Qiu et al., 2013b:48). If future discoveries confirm the in situ nature of proboscideans in Upper Aoerban, it would be an important biochronologic marker for northern Asia.

6.6. Palaeogale minuta

Palaeogale was known in the Oligocene of East Asia, such as the early Oligocene Hsanda Gol region (Lange-Badré and Dashzeveg, 1989; Matthew and Granger, 1924), late Oligocene Ulantatal area (Huang, 1982), and Saint-Jacques area in Inner Mongolia (Wang and Zhang, 2015). Bonis (1981) distinguished Miocene Palaeogale in its reduced and narrowed m2 and lost p1 and adopted the name P. minuta, which was also applied to the North American early Miocene forms. Given the European and North American records of P. minuta, Bonis speculated that Asia should record it, too. In the eastern-most European record, Palaeogale survived in the Greek island of Evia in the Aliveri fauna estimated to be MN 4 in age (Koufos, 2011, 2013).

In the Neogene of East Asia, following our initial report on Aoerban (Wang et al., 2009), Palaeogale was recorded in the earliest Miocene Suosuoquan assemblages II and III (~21.5–22.5 Ma) (Meng et al., 2013). We have also reported its presence in the early Miocene Gashunyinadege Fauna in Inner Mongolia (Qiu et al., 2013a).

The Aoerban Palaeogale morphology is consistent with Bonis' (1981) characterization of P. minuta, e.g., p1 absent (as in elsewhere, size variation is also large). The Lower Aoerban records of Palaeogale minuta (IVPP V25002 and V25004; Figs. 12A–E), together with that of Gashunyinadege, thus represent the last appearance of this species in Asia. The fact that it is well represented in the Lower Aoerban bed but absent in the Upper Aoerban signals that the Aoerban Formation probably captures the local extinction event (as opposed to effects of sample bias) for this small carnivoran.

6.7. Palaeogale?

A left jaw fragment with p4-m1 plus alveoli of c-p3 and m2 from near IM0407 (IVPP V25006; Figs. 12F, G) and a right jaw fragment with heavily worn m1 (IM1528) are probably closest to topotype materials of Palaeogale hyaenoides from the early Miocene German fissure fills of Wintershof-West (MN 3) (Dehm, 1950). A strongly double-keeled posterior face of the lower carnassial trigonid is consistent with assignment to Palaeogale. The protoconid keel is weaker than the metaconid keel (there is a bulge along the lower 2/3 of the keel but there is no discrete metaconid delineated by a notch, as is typically the case in carnivorans with a metaconid). However, its m1 (8.52 × 3.86 mm) is 23% longer than the mean m1 length (6.95 mm) of Wintershof-West sample (Dehm, 1950:table 16). Its p4 (6.01 × 2.91 mm), on the other hand, is about 10% shorter than its counterparts from Wintershof-West. In addition to these proportional differences, the p4 from Aoerban is also higher-crowned and has less development of the posterior accessory cusp than P. hyaenoides. This Aoerban form may represent a different species Palaeogale or a hypercarnivorous small feliform convergent to Palaeogale.

6.8. Stenogale sp.

A highly hypercarnivorous feliform from IM0711 is represented by two partial dentaries probably belonging to the same individual (IVPP

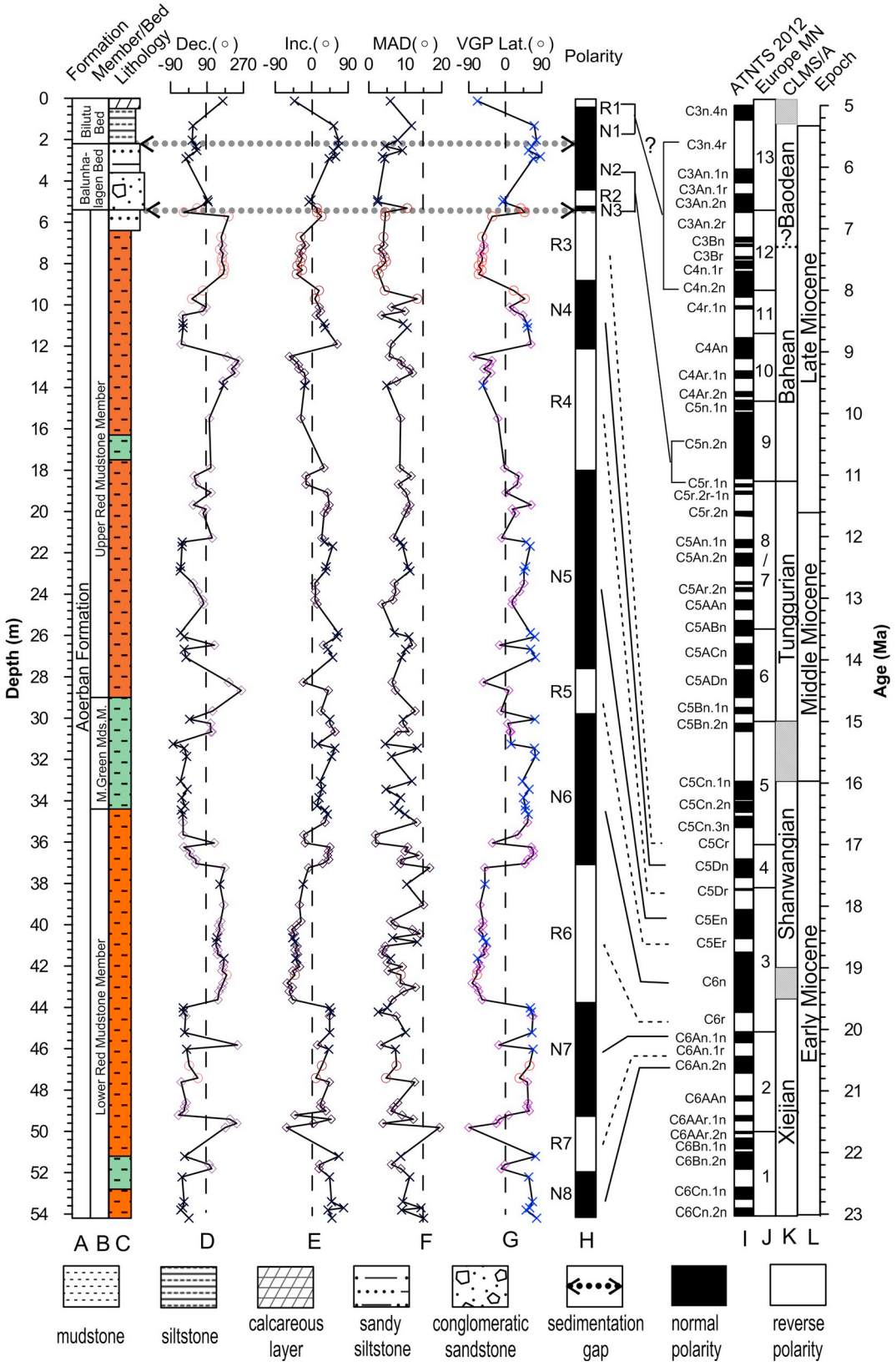

Fig. 9. Lithostratigraphy and magnetostratigraphy of the Aoerban sedimentary sequence. A&B, lithologic formations, members or beds; C, lithology; D, declination (Dec.); E, inclination (Inc.); F, maximum angular deviation (MAD); G, virtual geomagnetic pole (VGP) latitude; H, polarity zonation; I, the Astronomically Tuned Neogene Time Scale of Hilgen et al. (2012) (ATNTS2012); J, European Neogene Mammal (MN) units (Steininger, 1999); K, Chinese Land Mammal stages/ages (LMSs/As) (Qiu et al., 2013b); L, The Geologic Time Scale 2012 (Gradstein et al., 2012). Note that in D-G circles and diamonds represent thermally demagnetized specimens with ChRMs carried by hematite and magnetite, respectively; and crosses represent AF demagnetized specimens with ChRMs carried by magnetite.

V25007; Figs. 13A–D). This small feliform has an erect trigonid, a highly reduced m1 talonid dominated by a short hypoconid, a trenchant m2 with a single, centrally located cusp, presence of a m1 metaconid, and absence of p1. This combination of dental characters seems closest to the European Oligo-Miocene Stenogale. We follow Hunt Jr. (1998) in his summary of the characterization of this genus by Teilhard de Chardin (1915) based on the rich records from largely Oligocene Quercy fissures in France, supplemented by S. julieni from early Miocene St.-Gérand-le-Puy of France (Viret, 1929). As illustrated by Hunt Jr., (1998:fig. 6), among basal feliforms only the true felid, Proailurus, has become extremely hypercarnivorous and its m2 is so trenchant as to have lost all traces of tribosphenic molar pattern. In this regard, the

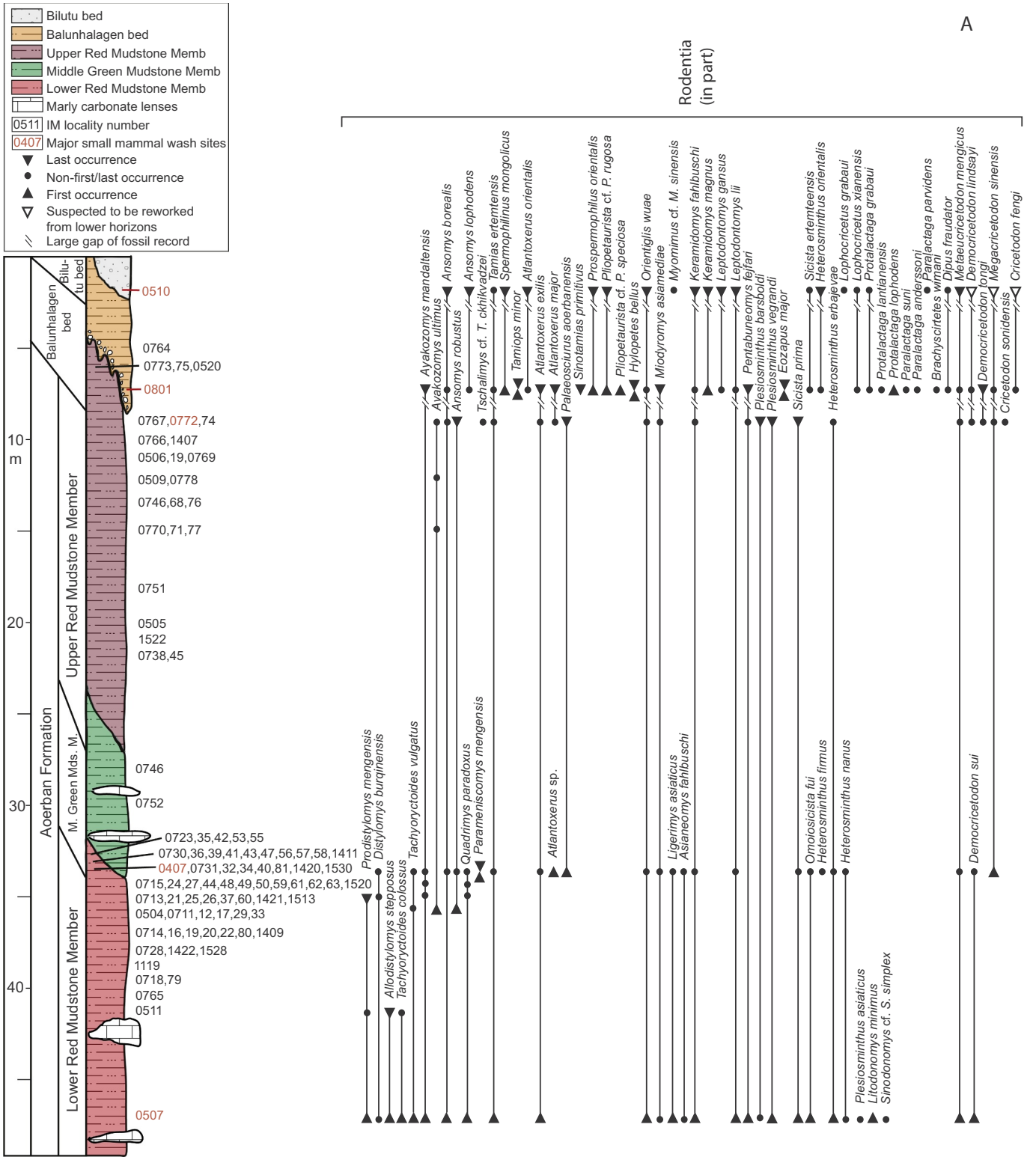

Fig. 10. (A and B). Biostratigraphy of fossil localities and taxa ranges. Relative stratigraphic position of individual localities are based on elevation data from Google Earth Pro (2015) and field observations. See Fig. 1 for map location of each localities and Table 1 for additional details of the localities.

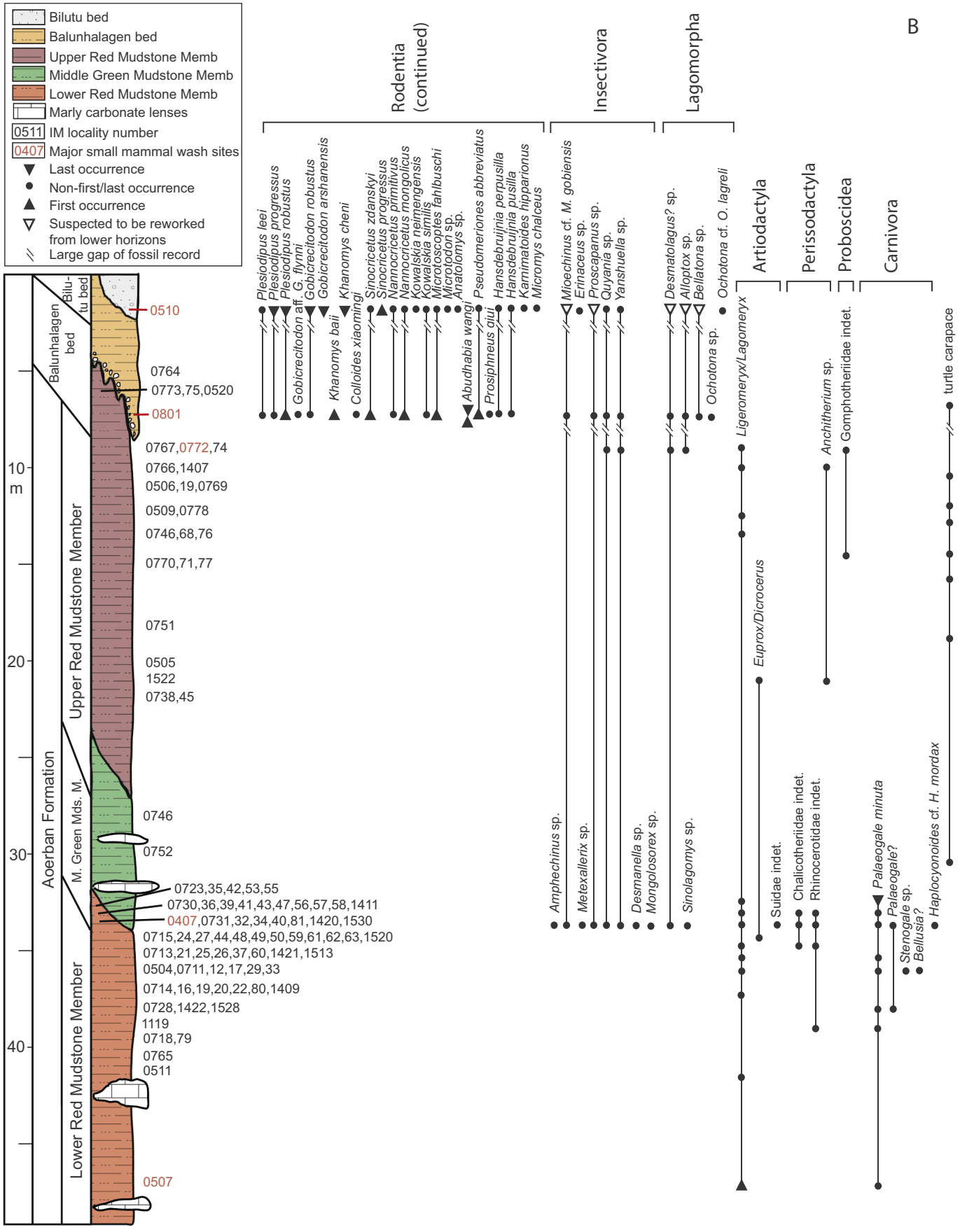

Fig. 10. (*continued*)

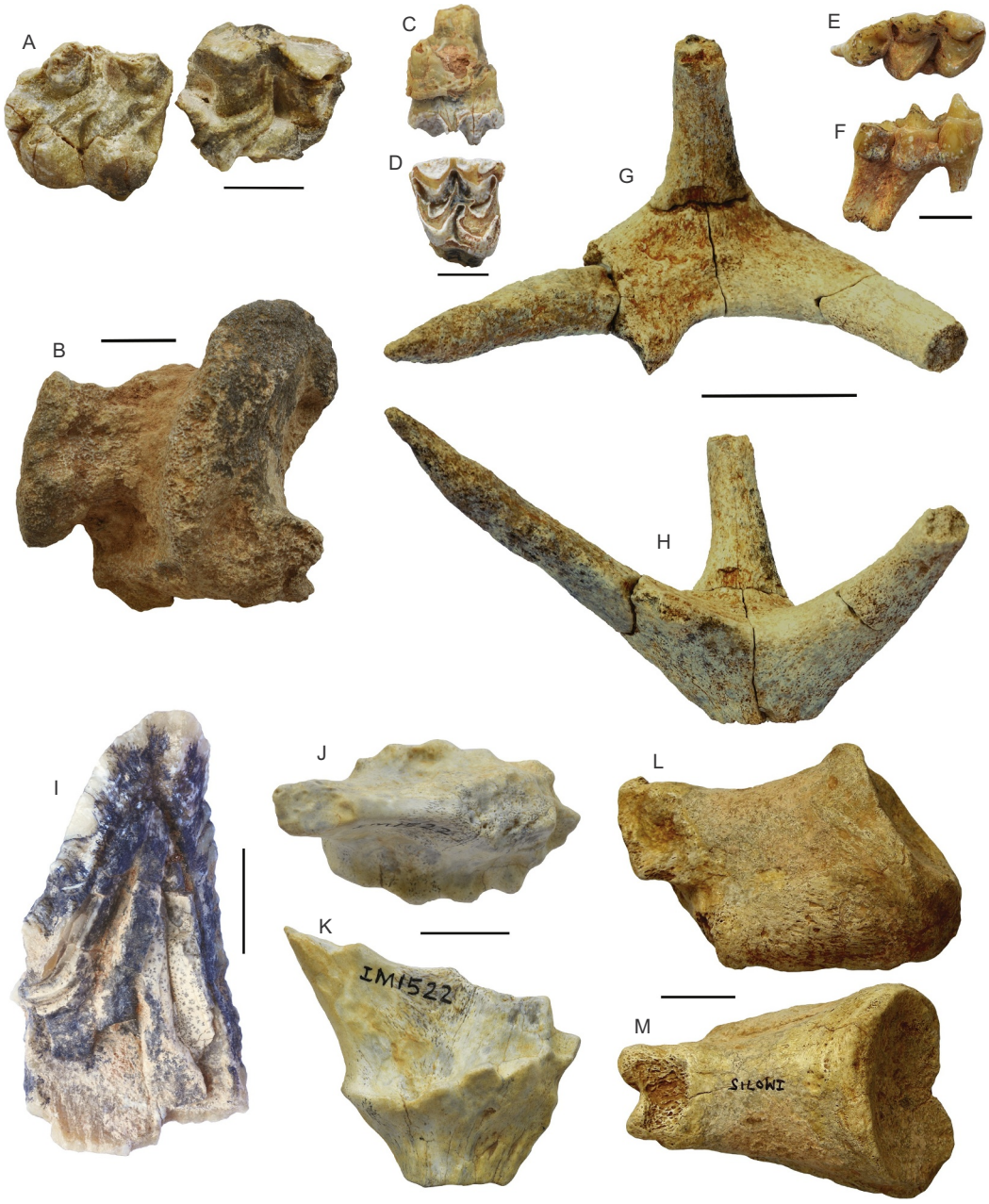

Fig. 11. Fossil horses, deers, proboscidean, and chalicothere from Aoerban Formation. *Anchitherium* sp.: A, two upper cheek teeth (IVPP V24989), and B, astragalus (IVPP V24990). *Ligeromeryx/Lagomeryx*: C, buccal, and D, occlusal views of an upper molar (IVPP V24991 from IM1511 loc); E, occlusal, and F, buccal views of right m3 (IVPP V24992 from IM0757 loc); G, dorsal, and H, lateral views of an antler (IVPP V24993 from IM0772 loc). Gomphotheriidae indet.: I, a fragment of a cheek tooth cusp (IVPP V24998 from IM0772 loc), internal view showing thick enamels. *Euprox* sp.: J, dorsal, and K, ventral views of an antler fragment (IVPP V24999 from IM1522 loc). Chalicotheriidae indet.: L, lateral, and M, dorsal views of a medial phalanx (IVPP V25001 from IM0715 loc). Scales for A, B, I, J, K are 10 mm; C, D, E, F are 5 mm; and G, H, L, M are 20 mm.

Aoerban Stenogale has reached a similar stage of evolution as Proailurus and its m2 has a single cusp. Hunt thus considered Stenogale a basal felid. However, Quercy S. gracilis retain a distinct trigonid in m2 and whether or not European Stenogale has a trenchant m2 by early Miocene is not clear. If our assignment of the Aoerban Stenogale is correct, it may represent a distinct Asian species. The Aoerban form is possibly related to a hypercarnivorous Asiavorator (Spassov and Lange-Badré, 1995). Lacking m2, Asiavorator cannot be easily compared but its m1 seems more primitive than the Aoerban form. Cryptailurus from Shimek's Quarry in early Miocene (Hemingfordian) of Nebraska (Martin and Lim, 2001) may also belong to this group.

6.9. *Ballusia?*

A left dentary fragment with a broken m1 (15.76 × 7.72 mm) from IM1409 is the only representative of this taxon (IVPP V25008; Figs. 13E–G). A broadened carnassial talonid is the most striking characteristic of this form, which is shared with Bellusia orientali from Shanwang, although the latter has a far broader talonid (Qiu et al., 1985). The Aoerban form is somewhat larger than the holotype of B. elmensis (m1 14 × 6 mm) from Elmer Tunnel site (Stehlin, 1917), the referred materials of B. elmensis from Wintershof-West (m1 length 13.7–15.0 mm) (Dehm, 1950), and holotype of B. orientali (m1 12.2 × 7.2 mm) from Shanwang. Based on the widening of the talonid,

Table 2
First appearance datum (FAD) and last appearance datum (LAD) of taxa from Aoerban Formation. Taxa that continue above local disconformity into the upper strata (Balunhalagen or Bilutu beds) are given a designation of " < 16.7 Ma" (upper limit of Aoerban Formation), indicating a lack of magnetic constraints for their LADs. Age calibrations are based on those in Table 1.

Taxa	FAD (Ma)	LAD (Ma)	Aoerban formation localities
Insectivora			
Amphechinus sp.	19.5	19.5	IM0407
Mioechinus cf. *M. gobiensis*	19.5	< 16.7	IM0407
Metexallerix sp.	19.5	19.5	IM0407
Proscapanus sp.	19.5	< 16.7	IM0407
Quyania sp.	19.5	< 16.7	IM0407, 0772
Yanshuella sp.	19.5	< 16.7	IM0407, 0772
Desmanella sp.	19.5	19.5	IM0407
Mongolosorex sp.	19.5	19.5	IM0407
Rodentia			
Prodistylomys mengensis	20.7	19.7	IM0507, 0511, 0721
Distylomys burqinensis	20.7	19.5	IM0407, 0507
Allodistylomys stepposus	20.7	20.4	IM0507, 0511
Tachyoryctoides colossus	20.7	20.4	IM0507, 0511
Tachyoryctoides vulgatus	20.7	19.7	IM0407, 0507, 0711
Ayakozomys mandaltensis	20.7	< 16.7	IM0407, 0507, 0511, 0711
Ayakozomys ultimus	19.7	< 16.7	IM0711, 0770, 0772, 0776, 0778
Ansomys borealis	20.7	< 16.7	IM0407, 0507, 0726, 0744, 0772
Ansomys robustus	19.5	16.7	IM0407, 0744, 0772
Tschalimys cf. *T. ckhikvadzei*	17.0	17.0	IM0772
Tamias ertemtensis	20.7	< 16.7	IM0407, 0507, 0772
Atlantoxerus exilis	20.7	< 16.7	IM0407, 0507, 0772
Atlantoxerus major	17.0	< 16.7	IM0772
Palaeosciurus aoerbanensis	19.5	17.0	IM0407, 0772
Orientiglis wuae	20.7	< 16.7	IM0407, 0507, 0772
Miodyromys asiamediae	20.7	< 16.7	IM0407, 0507, 0772
Ligerimys asiaticus	20.7	19.5	IM0407, 0507
Asianeomys fahlbuschi	20.7	19.5	IM0407, 0507
Keramidomys fahlbuschi	20.7	< 16.7	IM0407, 0507, 0772
Leptodontomys lii	20.7	< 16.7	IM0407, 0507
Pentabuneomys fejfari	20.7	< 16.7	IM0507, 0772
Plesiosminthus barsboldi	20.7	17.0	IM0407, 0507, 0772
Plesiosminthus vegrandi	20.7	17.0	IM0407, 0507, 0772
Plesiosminthus asiaticus	20.7	20.7	IM0507
Litodonomys minimus	20.7	20.7	IM0507
Sinodonomys cf. *S. simplex*	20.7	20.7	IM0507
Sicista prima	20.7	17.0	IM0407, 0507, 0772
Omoiosicista fui	20.7	19.5	IM0407, 0507
Heterosminthus firmus	19.5	19.5	IM0407
Heterosminthus erbajevae	20.7	17.0	IM0407, 0507, 0772
Metaeucricetodon mengicus	20.7	< 16.7	IM0407, 0507, 0772
Democricetodon sui	20.7	19.5	IM0407, 0507
Democricetodon lindsayi	17.0	< 16.7	IM0772
Democricetodon tongi	17.0	< 16.7	IM0772
Megacricetodon sinensis	19.5	< 16.7	IM0407, 0772
Cricetodon sonidensis	17.0	17.0	IM0772
Lagomorpha			
Desmatolagus? sp.	19.5	< 16.7	IM0407, 0772
Sinolagomys sp.	19.5	19.5	IM0407
Alloptox sp.	17.0	< 16.7	IM0772
Carnivora			
Palaeogale minuta	20.7	19.4	IM0407, 0507, 0701, 0712, 0718, 0721, 0728, 0755, 1411, 1422
Palaeogale?	19.9	19.5	IM0407, 1528
Stenogale sp.	19.7	19.7	IM0711
Bellusia sp.	19.8	19.8	IM1409
Haplocyonoides cf. *H. mordax*	19.5	19.5	IM1530
Artiodactyla			
Ligeromeryx/Lagomeryx	20.7	16.7	IM0507, 0511, 0520, 0716, 0739, 0742, 0753, 0757, 0760, 0767, 0772, 0773, 1407, 1411, 1420, 1513
Dicrocerus?	19.6	19.6	IM1520
Euprox sp.	18.5	18.5	IM1522
Suidae indet.	19.5	19.5	near IM0407
Perissodactyla			
Anchitherium sp.	18.5	17.2	IM1407, 1522
Chalicotheriidae indet.	19.6	19.5	IM0715, 0730, 0731, 0741, 0750
Rhinocerotidae indet.	20.1	19.4	IM0718, 0753
Proboscidea			
Gomphotheriidae indet.	17.8	17.0	IM0774, 0771

the Aoerban and Shanwang forms seem to belong to an East Asian clade distinct from those of western Europe. If this scenario is correct, the more primitive morphology of Aoerban species indicates an older age as compared to that of Shanwang.

7. Magnetostratigraphic correlation and geochronology

Given the robust biochronological constraints summarized above, the magnetozones determined for the Aoerban section can be readily correlated to the Astronomically Tuned Neogene Timescale of Hilgen et al. (2012) (ATNTS2012) (Fig. 9). Magnetozones R3–R7 and N4–N8 in the Aoerban Formation can be correlated to chrons C6An.2n through C5Cr with an age range of 20.71–16.72 Ma. The lower boundary of the Upper Red Mudstone Member at 29-m depth (Fig. 9C) is located within the lowest part of magnetozone R5 (27.6–29.8 m), which can be correlated to chron C5Er (Fig. 9H). The lower boundary of the Middle Green Mudstone Member at 34.4-m depth (Fig. 9C) is located within the lower part of magnetozone N6 (29.8–37.1 m), which can be correlated to chron C6n (Fig. 9H). Thus the lower boundary of the Upper Red Mudstone Member can be estimated to be 18.67 Ma by linear interpolation within chron C5Er; and the lower boundary of the Middle Green Mudstone Member can be estimated to be 19.36 Ma by linear interpolation within chron C6n.

Three magnetozones were determined in the Balunhalagen Bed: the upper (N2) and lower (N3) ones being normal; and the middle one (R2), reverse. However, due to the shortness of the section, truncated above by the Bilutu Bed, secure correlation of magnetozones R2 and N3 with the ATNTS2012 cannot be achieved. We tentatively correlate magnetozone N2 to chron C5n.

Two magnetozones were detected in the Bilutu Bed: the upper one (R1) being reverse; and the lower one (N1), normal. Once again, unequivocal correlation of the two magnetozones with the ATNTS2012 cannot be achieved due to the absence of unambiguous age-control points and the very short section.

Liddicoat et al. (2007) attempted a feasibility study on the magnetostratigraphy of the Aoerban section. They measured only 15 horizons in the section. Their results show that the section is of predominantly reverse polarity and only a short interval of normal polarity was found in the lower part of the section. The authors correlated the reverse polarity of the Aoerban section to the period near chron C5Dr or C6r. This test study tends to confuse rather than clarify matters. Wang et al. (2009) interpreted the normal polarity interval of Liddicoat et al.'s (2007) study as chron C6n, whereas Qiu et al. (2013) gave a somewhat different interpretation. Wang et al. (2009) pointed out that a much greater density is necessary for the Aoerban section to properly interpret the magnetic results, a deficiency remedied by this study with a sampling density more than one order of magnitude higher. Our

Fig. 12. Fossil carnivores from Aoerban Formation. *Palaeogale minuta*: A, stereophotos of occlusal view of left lower teeth, B, lingual view, and C, buccal view of left dentary (IVPP V25002 from IM0712 loc); D, buccal, and E, occlusal views of left P4 and maxillary fragment (IVPP V25004 from IM1422 loc). *Palaeogale*?: F, lingual view of left dentary, G, stereophotos of occlusal view of lower teeth (IVPP V25006 from IM0407 loc). Scales for D and E are 5 mm and those for the rest are 10 mm.

combined magnetobiochronology thus significantly refines the chronology of the terrestrial Aoerban Formation and associated faunas.

8. Faunas, biochrons, land mammal ages

During the past 30 years, great strides were made to expand the search in late Cenozoic strata of Inner Mongolia and to add many fossil sites filling in long gaps of records (Qiu, 1996; Qiu and Li, 2016; Qiu and Wang, 1999; Qiu et al., 2006; Qiu et al., 2013a). While the exquisite and abundant fossils are of great importance in faunal comparisons, their lack of stratigraphic context based on isolated strata presents an obstacle to age assessment.

Small mammals, particularly rodents, have played an important role in establishing relative age relationships in Inner Mongolia (Qiu and Li, 2016; Qiu and Wang, 1999; Qiu et al., 2006; Qiu et al., 2013a). In their latest monograph, Qiu and Li (2016) summarized the age relationship of small mammals in Aoerban strata as follows. The Lower Aoerban Fauna has eight families left over from the Oligocene, but 14 of its 27 rodent genera are found only in early Miocene of Eurasia, such as Ayakozomys, Tamias, Atlantoxerus, Ligerimys, Leptodontomys, Sicista, Democricetodon, and Megacricetodon. On the other hand, this fauna cannot be younger than early Miocene because it lacks common middle Miocene forms such as Sinotamias, Protalactaga, Plesiodipus, and Gobicricetodon. Based on rodents, Qiu and Li (2016) regard the Lower

Fig. 13. Fossil carnivores from Aoerban Formation. *Stenogale* sp. (IVPP V25007 from IM0711 loc): A, stereophotos of left jaw, B, stereophotos of right jaw, C, buccal view of left dentary, and D, lingual view of right dentary. *Ballusia* sp. (IVPP V25008 from IM1409 loc): E, stereophotos of left m1, F, buccal view, and G, lingual view of left dentary fragment. Scales are in 10 mm.

Aoerban Fauna as late Xiejian LMA. The overlying Upper Aoerban Fauna is less diverse (partly due to less screening at IM0772 locality) and shows somewhat more advanced characters with two new genera and nine new species, as well as the disappearance of archaic family Distylomyidae and further reduction, both in diversity and number of individuals, of Aplodontidae, Eomyidae, and Zapodidae. Qiu and Li (2016) considered the Upper Aoerban Fauna as late Shanwangian LMA.

As discussed above, the Lower Red Mudstone Member is magnetically dated to 20.71–19.36 Ma; the Middle Green Mudstone Member, 19.36–18.67 Ma; and the Upper Red Mudstone Member, 18.67–16.72 Ma. The Lower Aoerban Fauna, as defined by Wang et al. (2009), is represented by fossils from 65 localities (Table 1) that span much of the Lower Red Mudstone Member, including two small mammal localities (IM0407 and IM0507) with extensive screening, and the biostratigraphic range of this fauna roughly coincides with the Lower Red Mudstone Member. Accordingly, the Lower Aoerban Fauna is considered 20.71–19.36 Ma, corresponding to the late Xiejian Chinese LMA, or equivalent to the late MN2/early MN3 of the European mammal units. The Upper Aoerban Fauna, on the other hand, has fewer (23) localities and the main small mammal locality (IM0772) is near the top of the Upper Red Mudstone Member. As in the case of the Lower Aoerban Fauna, the Upper Aoerban Fauna was tentatively defined as

falling within the Upper Red Mudstone Member (Wang et al., 2009). The Upper Aoerban Fauna is thus dated as 18.67–16.72 Ma, corresponding to the Shanwangian Chinese LMA, or equivalent to the European mammal units from middle MN3 to early MN5.

Qiu et al. (2013b) noted that the Aoerban strata are likely the only fossil mammal section in China that straddles both Xiejian and Shanwangian LMAs. They further remarked that the first appearances of proboscideans, Megacricetodon, and Alloptox are potential candidates for defining the lower boundary of the Shanwangian. The Aoerban section contains all three. Proboscideans occur in the Upper Aoerban fauna (IM0771 and 0774), but represented by enamel fragments only, its taxonomy remains elusive. Based on this limited occurrence, the proboscidean biochron in Aoerban is 17.8–17.0 Ma (Table 2). Alloptox sp. from the Upper Aoerban fauna is currently under study, and produced in IM0772 locality only (17.0 Ma), although a denser sampling in lower strata may further refine its first appearance in the section. The lowest occurrence of Megacricetodon is at the top of the Lower Aoerban Red Mudstone (IM0407; FAD 19.5 Ma). Its absence in the lowest part of the member (i.e., IM0507) may suggest a true first appearance at IM0407 because IM0507 has been extensively screened.

Four other Aoerban taxa may be of chronologic importance. The Aoerban Palaeogale probably represents an Oligocene holdover, and the local (possibly East Asian) last appearance is 19.4 Ma. Aoerban appearance of the low-crowned horse, Anchitherium, is likely close to the earliest record in Asia, if not the entire Eurasia, with a local First Appearance Datum (FAD) of 18.5 Ma (Table 2). This record is important because immigrants are often preferable as powerful events for biochronology (Tedford et al., 1987; Woodburne, 2006). Abundant and diverse fossil deers in Aoerban section (currently under study), which represent the first occurrences of true cervids, may hold promise as another marker to characterize the Shanwangian Chinese LMA. However, fossils deers occur throughout the Aoerban Formation and the true first appearance in Asia likely predates its lowest occurrence in Aoerban. Finally, the bear dog Haplocyonoides cf. H. mordax (FAD 19.5 Ma) is comparable to those in European early Miocene (Wang et al., 2016), offering potential for refined age comparison when additional materials become available.

Of the three potential candidates (proboscideans, Megacricetodon, and Alloptox) for lower boundary of the Shanwangian LMA proposed by Z.-x. Qiu et al. (2013), none is well-studied enough to be selected for this purpose. Previous Chinese workers tended to directly equate this boundary with European Orleanian and/or Burdigalian (Deng et al., 2008; Li et al., 1984). Without clearly defining it, Z.-x. Qiu et al. (2013:fig. 1.4) placed the Xiejian/Shanwangian boundary somewhere between 19 and 19.5 Ma. Aoerban *Megacricetodon sinensis* (FAD 19.5 Ma) comes close to this range, but is currently represented by two isolated teeth only, which may either suggest its true first appearance with low frequency or a potential admixture from upper strata (Qiu and Li, 2016:431). Also noteworthy is the Anchitherium FAD (18.5 Ma), which, too, is represented by only two fragmentary cheek teeth and an astragalus, but seems likely a true early record.

However, when the lower boundary of the Shanwangian Chinese LMA is defined in the future, the Aoerban section can serve as a potential candidate because of its continuity and richness of fossils. With our integrated biostratigraphy and magnetochronology, this study is a step toward that direction.

9. Conclusions

The Aoerban area in central Inner Mongolia is an early-late Miocene vertebrate fossil site that produces rich and diverse mammals and fills a major gap in our knowledge about terrestrial early Miocene records of East Asia. Our field works during the past decade have documented a detailed record of lithostratigraphy, biostratigraphy, and magnetostratigraphy, which are presented here for the first time. Important First Appearance Datum (FAD) from the Aoerban strata includes true deers (Cervidae) with several types of shed antlers, low-crowned anchithere horse (Anchitherium), ancestral pika (Alloptox), cricetid rodent (Megacricetodon), and an indication of the earliest record of elephant ancestor (the Proboscidea event; Gomphotheriidae).

Faunas from the Aoerban Formation belong to the Xiejian to Shanwangian Chinese LMAs. With these biochronological constraints, magnetostratigraphy in the Aoerban Formation can be correlated to C6An.2n to C5Cr with an age range of 20.71–16.72 Ma of the ATNTS2012. Depending on how the boundary is defined, fossil mammals from the Aoerban are relevant in the discussions of the beginning of Shanwangian LMA as well as terminal records of Xiejian LMA. The Aoerban record will serve as a basis for studying mammalian evolution, biogeography, and paleoenvironment in the early Miocene of East Asia.

Acknowledgments

We thank field participants from Institute of Vertebrate Paleontology and Paleoanthropology, Chinese Academy of Sciences, Mr. Shen Wei from the Cultural Bureau of Sonid Zuoqi, and Mr. Wang Hongjiang from the Cultural Station of Xilinhot for their assistance during fieldwork. We greatly appreciate the support and advice by Qiu Zhuding, whose lifetime experience in Inner Mongolia has been invaluable for success in the field. We are also grateful for the hospitality and permission of the Jirimutu family, the landowners of the Aoerban field area. Paleomagnetic and mineral magnetic measurements were made in the Paleomagnetism and Geochronology Laboratory (PGL), Beijing. We thank Yanping Song for assistance in Photoshop manipulation of images. We are grateful to Yuri Kimura and Larry Flynn for their editorial efforts to improve this paper. We greatly appreciate the detailed edits in English language by Howard Falcon-Lang. Financial assistance was provided by Chinese Academy of Science Outstanding Overseas Scholar Fund (No. 2004-2-4), US National Science Foundation (EAR 0446699 and EAR 0716235), National Natural Science Foundation of China grants (41504058, 41690112 and 40730210), National Key Basic Research Program of China grants (2012CB821900 and 2006CB806400), and a Chinese Academy of Sciences grant (KZCX2-YW-120).

References

Azanza, B., Ginsburg, L., 1997. A revision of the large lagomerycid artiodactyls of Europe. Palaeontology 40, 461–485.
Bonis, L.d., 1981. Contribution a l'etude du genre *Palaeogale* Meyer (Mammalia, Carnivora). Ann. Paleontol. 67, 37–56.
Chow, M.-c., 1959. New species of fossil Proboscidea from South China. Acta Palaeontol. Sinica 7, 251–258.
Chow, M.-c., Hu, C.-k., 1956. The occurrence of *Anchitherium aurelianense* at Fangshan, Nanking. Acta Palaeontol. Sinica 4, 525–533.
Colbert, E.H., 1939. A new anchitheriine horse from the Tung Gur Formation of Mongolia. Am. Mus. Novit. 1019, 1–9.
Day, R., Fuller, M., Schmidt, V.A., 1977. Hysteresis properties of titanomagnetites: grainsize and compositional dependence. Phys. Earth Planet. Inter. 13, 260–267.
Dehm, R., 1950. Die Raubtiere aus dem Mittel-Miocän (Burgidalium) von Wintershof-West bei Eichstätt in Bayern. Bayer. Akad. Wiss. Math.-Natur. Kl. Abh. (N. F.) 58, 1–141.
Deng, C.-l., Zhu, R.-x., Jackson, M.J., Verosub, K.L., Singer, M.J., 2001. Variability of the temperature-dependent susceptibility of the Holocene eolian deposits in the Chinese loess plateau: a pedogenesis indicator. Phys. Chem. Earth Solid Earth Geod. 26, 873–878.
Deng, T., Wang, W.-m., Yue, L.-p., 2008. Report on research of the Shanwangian and Baodean Stages in the continental Neogene Series of China. In: Wang, Z.-j., Huang, Z.-g (Eds.), Reports on Establishing the Major Stages in China. Geological Publishing House, Beijing, pp. 13–31.
Deng, C.-l., He, H.-y., Pan, Y.-x., Zhu, R.-x., 2013. Chronology of the terrestrial Upper Cretaceous in the Songliao Basin, northeast Asia. Palaeogeogr. Palaeoclimatol. Palaeoecol. 385, 44–54.
Forstén, A., 1991. Size trends in Holarctic anchitherines (Mammalia, Equidae). J. Paleontol. 65, 147–159.
Google Earth Pro (Version 7.3.2.5487), 2015. Available from https://www.google.com/work/earthmaps/earthpro.html. Mountain View, CA: Google Inc.
Gradstein, F.M., Ogg, J.G., Schmitz, M.D., Ogg, G.M., 2012. A Geologic Time Scale 2012. Elsevier BV, Amsterdam, the Netherland.
Hilgen, F.J., Lourens, L.J., Van Dam, J.A., Beu, A.G., Foyes, A.F., Cooper, R.A., Krijgsman,

W., Ogg, J.G., Piller, W.E., Wilson, D.S., 2012. The Neogene Period. In: Gradstein, F.M., Ogg, J.G., Schmitz, M.D., Ogg, G.M. (Eds.), The Geologic Time Scale 2012, vol. 2. Elsevier, Amsterdam, pp. 923–978.
Huang, X.-s., 1982. Preliminary observation on the Oligocene stratigraphic section and on the fauna of the Wulantata'er area, Alxa Left Banner, Inner Mongolian Autonomous Region. Vert. PalAsiat. 20, 337–345.
Hunt Jr., R.M., 1998. Evolution of the aeluroid Carnivora: diversity of the earlier aeluroids from Eurasia (Quercy, Hsanda-Gol) and the origin of felids. Am. Mus. Novit. 3252, 1–65.
Jelinek, V., 1978. Statistical processing of anisotropy of magnetic-susceptibility measured on groups of specimens. Stud. Geophys. Geod. 22, 50–62.
King, J.W., Channell, J.E.T., 1991. Sedimentary magnetism, environmental magnetism, and magnetostratigraphy. U. S. National Report to International Union of Geodesy and Geophysics 1987–1990. Rev. Geophys. 29, 358–370.
Kirschvink, J.L., 1980. The least-squares line and plane and the analysis of paleomagnetic data. Geophys. J. R. Astron. Soc. 62, 699–718.
Koufos, G.D., 2011. The Miocene carnivore assemblage of Greece. Estud. Geol. 67, 291–320.
Koufos, G.D., 2013. Chapter 28. Neogene mammal biostratigraphy and chronology of Greece. In: Wang, X., Flynn, L.J., Fortelius, M. (Eds.), Fossil Mammals of Asia: Neogene Biostratigraphy and Chronology. Columbia University Press, New York, pp. 595–625.
Lange-Badré, B., Dashzeveg, D., 1989. On some Oligocene carnivorous mammals from Central Asia. Acta Palaeontol. Pol. 34, 125–148.
Li, C.-k., Lin, Y.-p., Gu, Y.-m., Hou, L.-h., Wu, W.-y., Qiu, Z.-d., 1983. The Aragonian vertebrate fauna of Xiacaowan, Jiangsu. 1. A brief introduction to the fossil localities and preliminary report on the new material. Vert. PalAsiat. 21, 313–327.
Li, C.-k., Wu, W.-y., Qiu, Z.-d., 1984. Chinese Neogene: subdivision and correlation [in Chinese with English abstract]. Vert. PalAsiat. 22, 163–178.
Liddicoat, J.C., Wang, X., Qiu, Z.-d., Li, Q., 2007. Recent palaeomagnetic and magnetostratigraphic investigations on and around the Tunggur Tableland, central Nei Mengol (Inner Mongolia). Vert. PalAsiat. 45, 110–117.
Lowrie, W., 1990. Identification of ferromagnetic minerals in a rock by coercivity and unblocking temperature properties. Geophys. Res. Lett. 17, 159–162.
Martin, L.D., Lim, J.-D., 2001. A musteliform carnivore from the American early Miocene. Neues Jb. Geol. Paläontol. Monat. 5, 265–276.
Matthew, W.D., Granger, W., 1924. New Carnivora from the Tertiary of Mongolia. Am. Mus. Novit. 104, 1–9.
Meng, J., Ye, J., Wu, W.-y., Ni, X.-j., Bi, S.-d., 2013. Chapter 3. A single-point base definition of the Xiejian age as an exemplar for refining Chinese land mammal ages. In: Wang, X., Flynn, L.J., Fortelius, M. (Eds.), Fossil Mammals of Asia: Neogene Biostratigraphy and Chronology. Columbia University Press, New York, pp. 124–141.
Miyata, K., Tomida, Y., 2010. *Anchitherium* (Mammalia, Perissodactyla, Equidae) from the early Miocene Hiramaki Formation, Gifu Prefecture, Japan, and its implication for the early diversification of Asian *Anchitherium*. J. Paleontol. 84, 763–773.
Qiu, Z.-d., 1996. Middle Miocene Micromammalian Fauna from Tunggur, Nei Mongol. Academic Press, Beijing.
Qiu, Z.-x., 1989. The Chinese Neogene mammalian biochronology — its correlation with the European Neogene mammalian zonation. In: Lindsay, E.H., Fahlbusch, V., Mein, P. (Eds.), European Neogene Mammal Chronology. Plenum Press, New York, pp. 527–556.
Qiu, Z.-d., Li, Q., 2016. Neogene rodents from central Nei Mongol, China. Palaeontol. Sinica N. Ser. C 198, 1–684.
Qiu, Z.-d., Qiu, Z.-x., 2013. Chapter 4. Early Miocene Xiejiahe and Sihong fossil localities and their faunas, eastern China. In: Wang, X., Flynn, L.J., Fortelius, M. (Eds.), Fossil Mammals of Asia: Neogene Biostratigraphy and Chronology. Columbia University Press, New York, pp. 142–154.
Qiu, Z.-x., Qiu, Z.-d., 1995. Chronological sequence and subdivision of Chinese Neogene mammalian faunas. Palaeogeogr. Palaeoclimatol. Palaeoecol. 116, 41–70.
Qiu, Z.-d., Wang, X., 1999. Small mammal faunas and their ages in Miocene of central Nei Mongol (Inner Mongolia). Vert. PalAsiat. 37, 120–139.
Qiu, Z.-x., Yan, D.-f., Jia, H., Wang, B.-z., 1985. Dentition of the Ursavus skeleton from Shanwang, Shandong Province. Vert. PalAsiat. 23, 264–275.
Qiu, Z.-d., Wang, X., Li, Q., 2006. Faunal succession and biochronology of the Miocene through Pliocene in Nei Mongol (Inner Mongolia). Vert. PalAsiat. 44, 164–181.
Qiu, Z.-x., Wang, B.-y., Xie, J.-y., 1998. Mid-Tertiary chalicothere (Perissodactyla) fossils from Lanzhou, Gansu, China. Vert. PalAsiat. 36, 297–318.
Qiu, Z.-d., Wang, X., Li, Q., 2013a. Chapter 5. Neogene faunal succession and biochronology of central Nei Mongol (Inner Mongolia). In: Wang, X., Flynn, L.J., Fortelius, M. (Eds.), Fossil Mammals of Asia: Neogene Biostratigraphy and Chronology. Columbia University Press, New York, pp. 155–186.
Qiu, Z.-x., Qiu, Z.-d., Deng, T., Li, C.-k., Zhang, Z.-q., Wang, B.-y., Wang, X., 2013b. Chapter 1. Neogene land mammal stages/ages of China — toward the goal to establish an Asian land mammal stage/age scheme. In: Wang, X., Flynn, L.J., Fortelius, M. (Eds.), Fossil Mammals of Asia: Neogene Biostratigraphy and Chronology. Columbia University Press, New York, pp. 29–90.
Roberts, A.P., Cui, Y.L., Verosub, K.L., 1995. Wasp-waisted hysteresis loops: mineral magnetic characteristics and discrimination of components in mixed magnetic systems. J. Geophys. Res. 100, 17909–17924.
Spassov, N., Lange-Badré, B., 1995. *Asiavorator altidens* gen. et sp. nov., un mammifère carnivore nouveau de l'Oligocène supérieur de Mongolie. Ann. Paleontol. 81, 109–123.
Stacey, F.D., Banerjee, S.K., 1974. The Physical Principles of Rock Magnetism. Elsevier, Amsterdam.
Stehlin, H.G., 1917. Miocäne Säugetierreste aus der Gegend von Elm (Prov. Hessen). Verh. Naturforsch. Ges. Basel 28, 191–205.
Steininger, F.F., 1999. Chronostratigraphy, geochronology and biochronology of the Miocene "European Land Mammal Mega-Zone" (ELMMZ) and the Miocene "Mammal-Zones (MN-Zones)". In: Rössner, G.E., Heissig, K. (Eds.), The Miocene Land Mammals of Europe. Dr. Friedrich Pfeil, Munich, pp. 9–24.
Tarling, D.H., Hrouda, F., 1993. The Magnetic Anisotropy of Rocks. Chapman and Hall, London.
Tassy, P., 1989. The "Proboscidean Datum Event": how many proboscideans and how many events? In: Lindsay, E.H., Fahlbusch, V., Mein, P. (Eds.), European Neogene Mammal Chronology. Plenum Press, New York, pp. 237–252.
Tauxe, L., 1998. Paleomagnetic principles and practice. In: Kluwer Academic Publishers. Dordrecht, Netherlands.
Tauxe, L., 2010. Essentials of Paleomagnetism. University of California Press, Berkeley.
Tedford, R.H., Galusha, T., Skinner, M.F., Taylor, B.E., Fields, R.W., Macdonald, J.R., Rensberger, J.M., Webb, S.D., Whistler, D.P., 1987. Faunal succession and biochronology of the Arikareean through Hemphillian interval (late Oligocene through earliest Miocene epochs) in North America. In: Woodburne, M.O. (Ed.), Cenozoic Mammals of North America. Geochronology and Biostratigraphy. University of California Press, Berkeley, pp. 153–210.
Teilhard de Chardin, P., 1915. Les carnassiers des Phosphorites du Quercy. Ann. Paleontol. 9, 101–191.
Verosub, K.L., Roberts, A.P., 1995. Environmental magnetism: past, present, and future. J. Geophys. Res. 100, 2175–2192.
Viret, J., 1929. Les faunes de mammifères l'Oligocène supérieur de la Limagne Bourbonnaise. Ann. Univ. Lyon Nouv. Ser. 47, 1–328.
Wang, B.-y., Qiu, Z.-x., 2002. A new species of Platybelodon (Gomphotheriidae, Proboscidea, Mammalia) from early Miocene of the Danghe area, Gansu, China. Vert. PalAsiat. 40, 291–299.
Wang, J., Zhang, Z.-q., 2015. Phylogenetic analysis on *Palaeogale* (Palaeogalidae, Carnivora) based on specimens from Oligocene strata of Saint-Jacques, Nei Mongol. Vert. PalAsiat. 53, 310–334.
Wang, X., Qiu, Z.-d., Li, Q., Tomida, Y., Kimura, Y., Tseng, Z.J., Wang, H.-j., 2009. A new early to late Miocene fossiliferous region in central Nei Mongol: lithostratigraphy and biostratigraphy in Aoerban strata. Vert. PalAsiat. 47, 111–134.
Wang, X., Wang, H.-j., Jiangzuo, Q.-g., 2016. New record of a haplocyonine amphicyonid in early Miocene of Nei Mongol fills a long-suspected geographic hiatus. Vert. PalAsiat. 54, 21–35.
Woodburne, M.O., 2006. Mammal ages. Stratigraphy 3, 229–261.
Young, C.-c., 1937. On a Miocene mammalian fauna from Shantung. Bull. Geol. Soc. China 17, 209–245.
Zijderveld, J.D.A., 1967. A.C. demagnetization in rocks: analysis of results. In: Collinson, D.W., Creer, K.M., Runcorn, S.K. (Eds.), Methods in Paleomagnetism. Elsevier, New York, pp. 254–286.